DNA-TR-85-296

NORMAL D-REGION MODELS FOR WEAPON EFFECTS CODE

Burt Gambill
Kaman Tempo
P. O. Drawer QQ
Santa Barbara, CA 93102

18 September 1985

Technical Report

CONTRACT No. DNA 001-82-C-0024

THIS WORK WAS SPONSORED BY THE DEFENSE NUCLEAR AGENCY
UNDER RDT&E RMSS CODE B322085466 S99QMXBC00130 H2590D.

Prepared for
Director
DEFENSE NUCLEAR AGENCY
Washington, DC 20305-1000

DISTRIBUTION LIST UPDATE

This mailer is provided to enable DNA to maintain current distribution lists for reports. We would appreciate your providing the requested information.

☐ Add the individual listed to your distribution list.

☐ Delete the cited organization/individual.

☐ Change of address.

NAME: _____

ORGANIZATION: _____

OLD ADDRESS	CURRENT ADDRESS
_____	_____
_____	_____
_____	_____

TELEPHONE NUMBER: ( ) _____

SUBJECT AREA(s) OF INTEREST:

_____	_____
_____	_____
_____	_____

DNA OR OTHER GOVERNMENT CONTRACT NUMBER: _____

CERTIFICATION OF NEED-TO-KNOW BY GOVERNMENT SPONSOR (if other than DNA):

SPONSORING ORGANIZATION: _____

CONTRACTING OFFICER OR REPRESENTATIVE: _____

SIGNATURE: _____

UNCLASSIFIED
SECURITY CLASSIFICATION OF THIS PAGE

AD-A171862

REPORT DOCUMENTATION PAGE

Form Approved
OMB No. 0704-0188
Exp. Date: Jun 30, 1986

1a. REPORT SECURITY CLASSIFICATION UNCLASSIFIED	1b. RESTRICTIVE MARKINGS
2a. SECURITY CLASSIFICATION AUTHORITY N/A since Unclassified	3. DISTRIBUTION/AVAILABILITY OF REPORT Approved for public release; distribution is unlimited.
2b. DECLASSIFICATION/DOWNGRADING SCHEDULE N/A since Unclassified	
4. PERFORMING ORGANIZATION REPORT NUMBER(S) KT-85-038(R)	5. MONITORING ORGANIZATION REPORT NUMBER(S) DNA-TR-85-296
6a. NAME OF PERFORMING ORGANIZATION Kaman Tempo 6b. OFFICE SYMBOL (If applicable)	7a. NAME OF MONITORING ORGANIZATION Director Defense Nuclear Agency
6c. ADDRESS (City, State, and ZIP Code) P. O. Drawer QQ Santa Barbara, CA 93102	7b. ADDRESS (City, State, and ZIP Code) Washington, DC 20305-1000
8a. NAME OF FUNDING/SPONSORING ORGANIZATION 8b. OFFICE SYMBOL (If applicable)	9. PROCUREMENT INSTRUMENT IDENTIFICATION NUMBER DNA 001-82-C-0024
8c. ADDRESS (City, State, and ZIP Code)	10. SOURCE OF FUNDING NUMBERS PROGRAM ELEMENT NO: 62715H; PROJECT NO: S99QMXB; TASK NO: C; WORK UNIT ACCESSION NO: DH008352

11. TITLE (Include Security Classification)
NORMAL D-REGION MODELS FOR WEAPON EFFECTS CODES

12. PERSONAL AUTHOR(S)
Gambill, B.

13a. TYPE OF REPORT	13b. TIME COVERED	14. DATE OF REPORT (Year, Month, Day)	15. PAGE COUNT
Technical	FROM 850101 TO 850824	850918	68

16. SUPPLEMENTARY NOTATION
This work was sponsored by the Defense Nuclear Agency under RDT&E RMSS Code B322085466 S99QMXBC00130 H2590D.

17. COSATI CODES			18. SUBJECT TERMS (Continue on reverse if necessary and identify by block number)
FIELD	GROUP	SUB-GROUP	
4	1		Reflection Coefficient; Normal D-Region Models; Electron Concentration; Propagation Losses; Vertical Gradient; Diurnal Variation; D-Region
20	14		

19. ABSTRACT (Continue on reverse if necessary and identify by block number)

This report examines several normal D-region models and their application to VLF/LF propagation predictions. Special emphasis is placed on defining models that reproduce measured normal propagation data and also provide reasonable departure/recovery conditions after an ionospheric disturbance. An interim numerical model is described that provides for selection of a range of normal D-region electron profiles and also provides for a smooth transition to disturbed profiles. Requirements are also examined for defining prescribed D-region profiles using complex aero-chemistry models.

20. DISTRIBUTION/AVAILABILITY OF ABSTRACT ☐ UNCLASSIFIED/UNLIMITED ☒ SAME AS RPT ☐ DTIC USERS	21. ABSTRACT SECURITY CLASSIFICATION UNCLASSIFIED
22a. NAME OF RESPONSIBLE INDIVIDUAL Betty L. Fox	22b. TELEPHONE (Include Area Code) (202) 325-7042 22c. OFFICE SYMBOL DNA/STTI

DD FORM 1473, 84 MAR 83 APR edition may be used until exhausted
All other editions are obsolete

SECURITY CLASSIFICATION OF THIS PAGE
UNCLASSIFIED

SUMMARY

This report examines D-region models that are widely used to predict the performance of military communication systems. Four types of models, selected for this study, are described in Section 2. These are models based, respectively, on measured electron concentration profiles, physical representation of normal ion production sources and associated atmospheric chemistry models, inferences from VLF/LF propagation data, and prediction of the D-region absorption of electromagnetic waves in the HF band.

Results produced by the various model approaches are in reasonable agreement for the daytime D-region. Model adjustments to produce agreement among the results for daytime conditions can be easily made within allowable limits of parameter uncertainties of any of the models. Results produced for the nighttime D-region are not in good agreement. In general models based on electron concentration measurements, and those based on production rate and chemistry predict higher electron concentration in the 75 to 90 km altitude range than do those inferred from VLF/LF propagation measurements.

In Section 3, the rationale for adjusting profiles to match propagation data are discussed and parameter adjustments to produce profiles similar to those inferred from the VLF/LF propagation data are examined. A numerical procedure is defined for selection of normal profiles to provide for smooth transition from the selected normal to a disturbed profile. This procedure is applicable to simple models which use fixed reaction rates and assume a quasi-equilibrium solution to the deionization equations. The sensitivity of nighttime D-region profiles to variations in ion production rates and atmospheric reaction rates in more complex chemistry models is also examined. This sensitivity analysis indicates that the adjustments to reduce electron concentration cannot be obtained with changes in production rates and identifies the required changes in effective lumped-parameter chemistry reaction rates that would be required to match profiles inferred from propagation data. The required changes appear to be within allowable model limits. However, consistent changes in atmospheric constituents associated with the change in reaction

rates may have model implications for other systems or applications. The methods of implementing changes in the chemistry models are not defined.

The emphasis in Section 3 is placed on noon and midnight profiles. An important problem not addressed is day/night transition. The transition problem is another example where apparent discrepancies exist between empirical models and models inferred from propagation data. The empirical models show a very gradual transition. Propagation models show more abrupt transition. This is indicated by modal interference and signal phase variations measured as the day-night terminator moves along a propagation path.

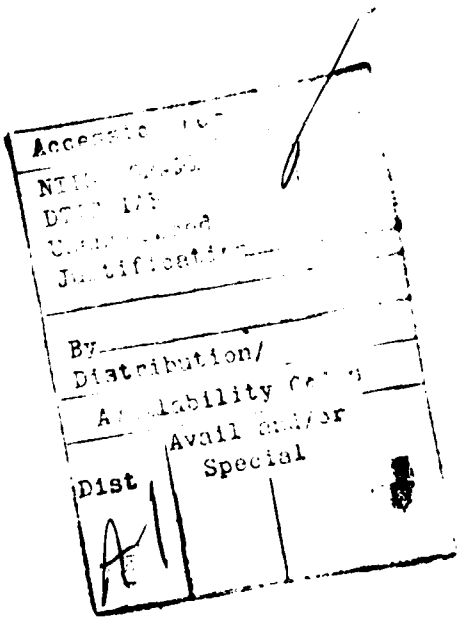

CONVERSION TABLE

Conversion factors for U.S. Customary to metric (SI) units of measurement.

MULTIPLY →	BY →	TO GET
TO GET ←	BY ←	DIVIDE

angstrom	1.000 000 X E -10	meters (m)
atmosphere (normal)	1.013 25 X E +2	kilo pascal (kPa)
bar	1.000 000 X E +2	kilo pascal (kPa)
barn	1.000 000 X E -28	meter^2 (m^2)
British thermal unit (thermochemical)	1.054 350 X E +3	joule (J)
calorie (thermochemical)	4.184 000	joule (J)
cal (thermochemical)/cm^2	4.184 000 X E -2	mega joule/m^2 (MJ/m^2)
curie	3.700 000 X E +1	giga becquerel (GBq)*
degree (angle)	1.745 329 X E -2	radian (rad)
degree Fahrenheit	t_K=(t°f+459.67)/1.8	degree kelvin (K)
electron volt	1.602 19 X E -19	joule (J)
erg	1.000 000 X E -7	joule (J)
erg/second	1.000 000 X E -7	watt (W)
foot	3.048 000 X E -1	meter (m)
foot-pound-force	1.355 818	joule (J)
gallon (U.S. liquid)	3.785 412 X E -3	meter^3 (m^3)
inch	2.540 000 X E -2	meter (m)
jerk	1.000 000 X E +9	joule (J)
joule/kilogram (J/kg) (radiation dose absorbed)	1.000 000	Gray (Gy)**
kilotons	4.183	terajoules
kip (1000 lbf)	4.448 222 X E +3	newton (N)
kip/inch^2 (ksi)	6.894 757 X E +3	kilo pascal (kPa)
ktap	1.000 000 X E +2	newton-second/m^2 (N-s/m^2)
micron	1.000 000 X E -6	meter (m)
mil	2.540 000 X E -5	meter (m)
mile (international)	1.609 344 X E +3	meter (m)
ounce	2.834 952 X E -2	kilogram (kg)
pound-force (lbf avoirdupois)	4.448 222	newton (N)
pound-force inch	1.129 848 X E -1	newton-meter (N•m)
pound-force/inch	1.751 268 X E +2	newton/meter (N/m)
pound-force/foot^2	4.788 026 X E -2	kilo pascal (kPa)
pound-force/inch^2 (psi)	6.894 757	kilo pascal (kPa)
pound-mass (lbm avoirdupois)	4.535 924 X E -1	kilogram (kg)
pound-mass-foot^2 (moment of inertia)	4.214 011 X E -2	kilogram-meter^2 (kg•m^2)
pound-mass/foot^3	1.601 846 X E +1	kilogram/meter^3 (kg/m^3)
rad (radiation dose absorbed)	1.000 000 X E -2	Gray (Gy)**
roentgen	2.579 760 X E -4	coulomb/kilogram (C/kg)
shake	1.000 000 X E -8	second (s)
slug	1.459 390 X E +1	kilogram (kg)
torr (mm Hg, 0°C)	1.333 22 X E -1	kilo pascal (kPa)

* The becquerel (Bq) is the SI unit of radioactivity; 1 Bq = 1 event/s.
**The Gray (Gy) is the SI unit of absorbed radiation.

TABLE OF CONTENTS

LIST OF ILLUSTRATIONS

LIST OF ILLUSTRATIONS (Concluded)

LIST OF TABLES

SECTION 1
INTRODUCTION

The D region, in the context of this report, includes the altitude range from about 40 to 100 km altitude. There are many applications for models of electron density in the undisturbed D region and as many models as there are applications. For computer codes that predict the effects of nuclear disturbance on the propagation of electromagnetic signals, the normal models provide the departure conditions and eventual recovery conditions of the ionosphere. While the nuclear effects models are not intended to be used for undisturbed predictions, reasonable models are required to provide for predictions of effects of weak disturbances and for estimates of recovery times. In addition, the nuclear effects codes suffer from a decrease in credibility when field strength predictions for non-disturbed or recovery conditions disagree with observed propagation data. Current normal ionosphere models in nuclear effects codes produce propagation losses larger than inferred from measured data. This discrepancy provided the impetus for this effort.

In this report, widely used models are discussed, showing similarities and differences and illustrating sometimes conflicting model requirements for obtaining generally applicable models for nuclear effect predictions. A numerical model approach is described that can provide some flexibility in a choice of normal ionosphere models. This revised model can be implemented in the SIMBAL code (Reference 1) for VLF and LF predictions. Implementation in models with complex chemistry calculations (such as WEDCOM, Reference 2) is discussed but the procedure is much more difficult.

Four types of models will be discussed. These are:

1. Hypothetical models which can be numerically specified and which can be used to reproduce detailed VLF and LF propagation data.
2. Empirical models derived from direct measurement of electron and ion density profiles.
3. Physical models based on models of normal ion-pair production sources and atmospheric chemistry models. This type of model is required for

nuclear effects codes, since the weapon-produced disturbances are modelled as additional ion-pair production sources and, in some cases, the disturbance changes atmospheric constituents and reaction rates.

4. Empirical models that reproduce observed values of D-region absorption of EM waves in the HF band.

In general, defining D-region models to reproduce VLF and LF propagation data is more difficult than defining models to reproduce HF absorption. VLF and LF reflection from the ionosphere depends on both the electron (and sometime heavy ion) concentration and vertical gradient. HF absorption is an integration of losses through the D region and can be reproduced by various vertical profiles. Both electrons and heavy ions can be important for VLF and LF, although ions usually have little effect for undisturbed conditions. In this report the D region will be characterized by electrons $N_e(h)$, representative posicive and negative ions $N_+(h)$ and $N_-(h)$, electron-neutral collision frequency $\nu_e(h)$ and average ion-neutral collision frequency $\nu_i(h)$.

Table 1 lists collision frequencies that have been used in this report.

The important altitude band where the D-region electron concentration and gradient are important for VLF/LF reflection has been addressed by several researchers. The reflecting region is defined in terms of the square of the index of refraction, n^2, where

$$n^2 = 1 - A(h) - jB(h) \qquad (1)$$

$$j = \sqrt{-1}$$

$$A(h) = A_e(h) + A_i(h)$$

$$B(h) = B_e(h) + B_i(h)$$

$$A_e(h) = \frac{3.18 \times 10^4 N_e(h)(\omega \pm \omega_{me})}{\omega\left[(\omega \pm \omega_{me})^2 + \nu_i^2(h)\right]}$$

Table 1. Electron-neutral and ion-neutral collision frequencies.

Altitude (km)	Electron-Neutral Collision Frequency (ν_e) s^{-1}	Ion-Neutral Collision Frequency (ν_i) s^{-1}
5	8.08E+10	3.37E+09
10	3.97E+10	1.75E+09
15	1.82E+10	8.30E+08
20	8.22E+09	3.75E+08
25	3.74E+09	1.69E+08
30	1.73E+09	7.72E+07
35	8.19E+08	3.57E+07
40	4.05E+08	1.72E+07
45	2.08E+08	8.60E+06
50	1.10E+08	4.50E+06
55	5.86E+07	2.77E+06
60	3.05E+07	1.69E+06
65	1.54E+07	1.01E+06
70	7.52E+06	5.79E+05
75	3.53E+06	3.21E+05
80	1.58E+06	1.70E+05
85	6.82E+05	8.58E+04
90	2.91E+05	4.19E+04
95	1.27E+05	2.06E+04
100	5.75E+04	1.06E+04

$$A_i(h) = \frac{5.45 \times 10^4 N_i(h)}{\omega^2 + \nu_i^2(h)}$$

$$B_e(h) = \frac{\nu_e(h)}{\omega \pm \omega_{me}} A_e(h)$$

$$B_i(h) = \frac{\nu_i(h)}{\omega} A_i(h)$$

where

ω_{me} is the electron gyrofrequency.

Field and Engel (Reference 3) showed that when $B(h) >> A(h)$ reflection maximizes at h_r, where h_r is defined by

$$B(h_r) = \sqrt{2} \cos^2 \phi_i \qquad (2)$$

and

ϕ_i = real angle of incidence.

Booker, Fejer, and Lee (Reference 4) extended the analysis to include variations in both $A(h)$ and $B(h)$ and defined the altitude h_r to be where

$$m(h_r) = \cos^2 \phi_i \ . \qquad (3)$$

In Equation 3

$$m(h) = \frac{2\ M(h)}{\left(8 + \cos^2 \psi_i\right)^{1/2} - \cos \psi_i} \ , \qquad (4)$$

$$M(h) = \left(A^2(h) + B^2(h)\right)^{1/2} \qquad (5)$$

and

$$\psi_i = \tan^{-1} (B(h)/A(h)) \quad . \tag{6}$$

Note that Equation 3 reduces to Equation 2 when $B(h) >> A(h)$.

Figure 1a shows the electron concentration as a function of altitude that satisfies Equation 3 for frequencies of 20 and 100 kHz and ϕ_i = 80 degrees. Values are shown with and without the effects of the magnetic field. The approximate formulas are not strictly valid when magnetic field effects are strong. These curves can be used to approximate the altitude range where D-region profiles must match prescribed profiles to match propagation data.

Figure 1b shows the concentration of ions required to satisfy Equation 3 for the same conditions.

Numerical calculations (Reference 5) which evaluated the altitude variation of the magnitude of downcoming waves reflected from various ionospheres tended to verify Equations 2 through 5. The reflecting region is thin and well defined when the vertical gradient of the electron concentration is large. When the gradient is small, the reflection region is thick and the numerical results indicated that reflections come from a somewhat lower altitude than Equations 2 or 3 predict.

Numerical evaluation of the reflection region for selected specific profiles is presented in Section 3.

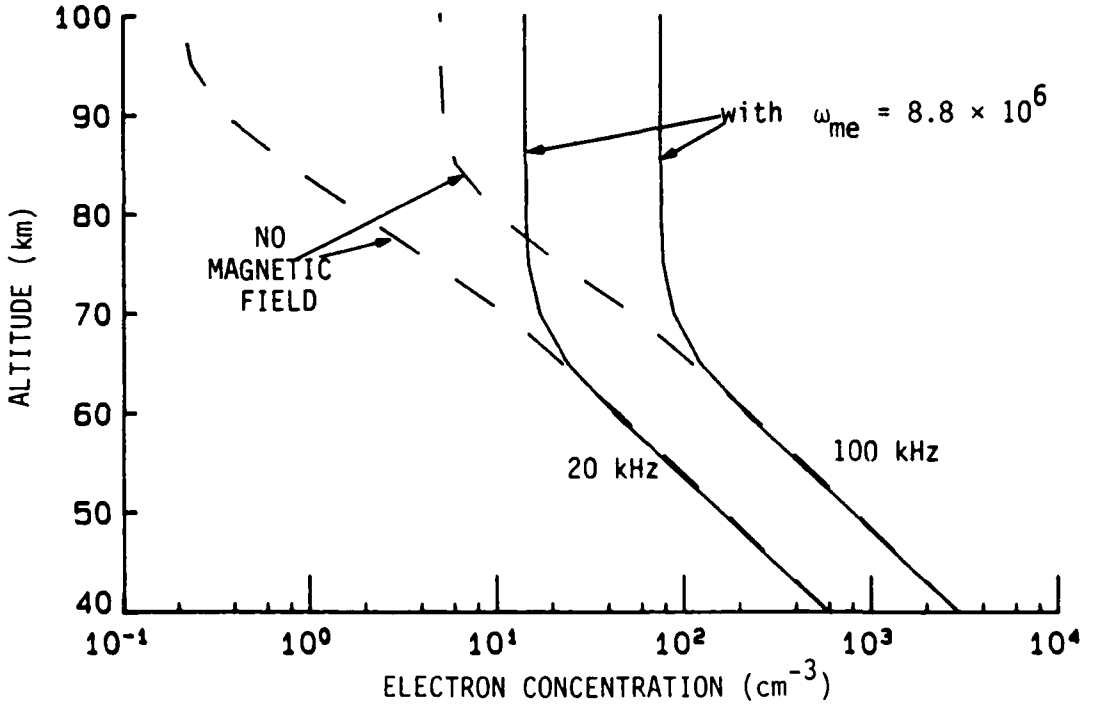

Figure 1a. Electron concentration to produce significant reflection for 20 and 100 kHz.

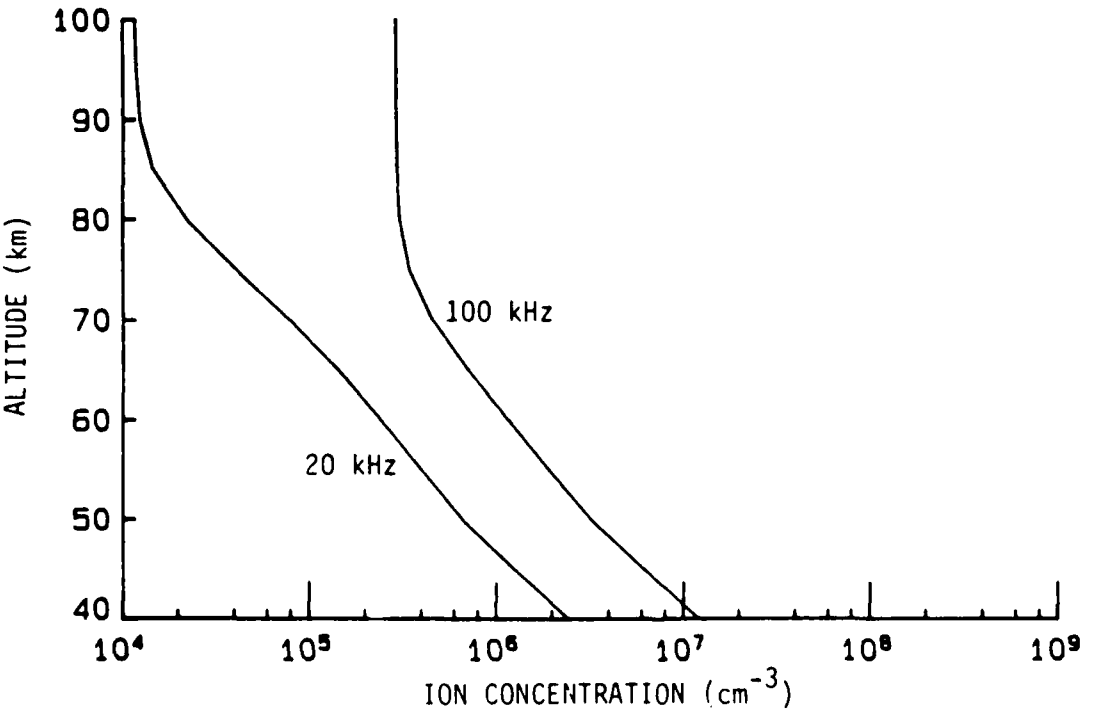

Figure 1b. Ion concentration to produce significant reflection for 20 and 100 kHz.

SECTION 2
WIDELY USED D-REGION MODELS

This report considers D-region models that are currently used widely in predictions of the performance of military systems in a disturbed environment. It is not intended to be a tutorial review of models. Four different types of models are discussed.

2.1 PROFILES TO MATCH VLF/LF PROPAGATION DATA.

Morfitt (Reference 6) and others have performed extensive comparisons of measured VLF/LF field strength values with detailed predictions. The procedure is to assume an electron concentration profile of the form

$$N_e(h) = 1.43 \times 10^7 \exp(-\beta h_w) \exp\left[(\beta - 0.15)h\right] \qquad (6)$$

and perform calculation for various values of h_w and β. For selected h_w and β the computed and measured field strength values (measured field strength as a function of distance between the transmitter and receiver) show remarkable agreement, including the location of peaks and nulls produced by constructive and destructive mode interference.

Tables 2, 3, and 4 from Reference 6 show values of β and h_w that produce a best fit to measured data for several frequencies and for daytime and nighttime conditions. The implied frequency dependence of the ionosphere cannot be real. The changes with frequency may occur because the altitude of maximum reflection moves upward with increasing frequency, thus waves of different frequencies are affected by different segments of the ionosphere profile. Selected profiles ($\beta = 0.3$, $h_w = 72$ for daytime and $\beta = 0.7$, $h_w = 88$ for nighttime) are used for reference and comparisons in later subsections.

Table 2. Effective electron density profiles for use in propagation predictions, midlatitude - Pacific. (Source: Reference 6)

Daytime		Nighttime	
Frequency (kHz)	Profile β (km^{-1}), h_w (km)	Frequency (kHz)	Profile β (km^{-1}), h_w (km)
Winter		Winter	
9 - 60	$\beta = 0.3$, $h_w = 74$	below 10	$\beta = 0.3$, $h_w = 87$
		10 - 15	$\beta = 0.4$, $h_w = 87$
		15 - 25	$\beta = 0.5$, $h_w = 87$
Summer		25 - 30	$\beta = 0.6$, $h_w = 88$
16 - 26	$\beta = 0.5$, $h_w = 70$	30 - 40	$\beta = 0.7$, $h_w = 88$
		40 - 60	$\beta = 0.8$, $h_w = 88$

Table 3. Best-fit exponential electron density profiles - nighttime winter data recorded aboard an aircraft, Hawaii to Southern California propagation path. (Source: Reference 6).

Hawaii Transmitter							
	7 February 1969			30 January 1974		1 February 1974	
kHz	β (km^{-1})	h_w (km)	kHz	β (km^{-1})	h_w (km)	β (km^{-1})	h_w (km)
9.340	0.35	87	9.340	0.3	87	0.3	89
10.897	0.4	87	10.897	0.4	87	0.3	89
14.010	0.5	87	15.567	0.5	86	0.4	88
15.567	0.5	87	21.794	0.7	87	0.5	88
17.124	0.5	87	28.020	1.0	88	0.5	89
21.794	0.5	88	37.361	1.0	88	0.6	88
24.908	0.5	88	40.475	1.2	88	0.6	88
26.464	0.5	88	46.702	1.2	88	0.7	88
28.020	0.5	88	52.929	1.2	88	0.7	88
31.134	0.6	88	56.042	1.2	88	0.7	88

Table 4. Best-fit exponential electron density profiles -- daytime winter data recorded aboard an aircraft, Hawaii to Southern California propagation path. (Source: Reference 6).

	Hawaii Transmitter				Sentinel Transmitter		
	2 February 1974		2 February 1974			2 February 1974	
kHz	β (km^{-1})	h_w (km)	β (km^{-1})	h_w (km)	kHz	β (km^{-1})	h_w (km)
9.340	0.3	72	0.3	75	9.336	0.3	74
10.897	0.3	72	0.3	75	14.003	0.3	74
15.567	0.3	72	0.3	75	17.115	0.3	74
21.794	0.3	72	0.3	75	24.895	0.3	74
28.020	0.3	73	0.3	75	28.007	0.3	74
37.361	0.35	73	0.3	75	34.231	0.3	74
40.475	0.35	73	0.3	75	38.898	0.3	74
46.702	0.35	73	0.3	75	43.566	0.3	74
52.929	0.35	73	0.3	75	49.790	0.3	75
56.042	0.35	73	0.3	75	56.104	0.3	75

2.2 MODELS BASED ON MEASUREMENTS OF ELECTRON DENSITY PROFILES.

2.2.1 Berry's Model.

Berry (Reference 7) analyzed a large number of experimentally determined vertical electron profiles and sought a model that would be useful for VLF and LF predictions. Following the lead of Morfitt and others at NOSC (Reference 6), who match propagation data using electron profiles with an exponential altitude variation, Berry also devised a model of the form

$$N(h_w) = N_o \exp -\beta(h_w - h_r) \qquad (7)$$

where β is chosen to fit the slope of measured data at the altitude h_r, and h_r is the altitude where Equation 2 is satisfied, using a frequency of 30 kHz and an angle of incidence of 81°. N_o is defined to make h_w and β consistent with the entries in Tables 2, 3, and 4.

The parameters used in the fit were

X_1 = cos χ (χ is the solar zenith angle)

X_2 = cos θ (θ is the geographic latitude)

X_3 = cos ϕ (ϕ = (m - 0.5)/12 × 2π, m = month)

X_4 = SSN (SSN is the smoothed Zurich sunspot number)

X_5 = absorption index (0 for quiet conditions, 1 for disturbed conditions).

The equations for the parameters are

$$h_w = 71.81 - 7.84X_1 + 8.04X_2 - 1.23X_3 - 0.0371X_4 - 7.03X_5 \quad (8)$$

$$\beta = 0.353 - 0.120X_1 + 0.072X_3 + 0.171X_5 \ . \quad (9)$$

Table 5 shows values of β and h_w for a latitude of 40 degrees, and various seasons, sunspot numbers, and times. Examples of Berry's results integrated with a physical model of the ionosphere are also shown in the next subsection. It can be seen that the nighttime reference altitudes are usually lower than the reference altitude used to match propagation data (Tables 2, 3, and 4). This may in part reflect the difficulty of making electron concentration measurements at the low concentrations that are important for VLF/LF propagation in the 75 to 85 km altitude range at night.

Table 5. Examples of altitude and slope parameters from Berry's model (quiet conditions).

Season	Local Time	SSN	h_w	β	h_r
Summer	1200	10	71.2	.31	59.6
(July)		100	67.9	.31	56.2
	0000	10	82.2	.48	74.7
		100	78.9	.48	71.1
Winter	1200	10	72.9	.23	57.1
(January)		100	69.6	.23	53.8
	0000	10	83.8	.40	74.7
		100	80.5	.40	71.5

2.2.2 McNamara's Model.

McNamara (Reference 8) extended the sets of profiles examined by Berry (Reference 7) and developed a numerical model of the electron density at heights of 55 to 90 km in 5-km steps. The model form is

$$\log_{10}(N_e) = a + b \cdot x\ (\text{zenith angle}) + c \cdot x\ (\text{latitude}) + d \cdot x\ (\text{solar activity}) + e \cdot x\ (\text{season}) + f \cdot x\ (\text{magnetic index}) \qquad (10)$$

where a, b, c, d, e, and f are constants derived for the fit and the x's provide the functional dependence on the independent variables. McNamara experimented statistically with different functional forms. The forms used to derive values for the constants are:

$$x\ (\text{zenith angle}, \psi) = \cos \psi ,$$

$$x\ (\text{latitude}, \theta) = \sin 2\theta , \quad h \geq 75 \text{ km}$$
$$= 0. + 0.9 \sin^4 \theta , \quad h \leq 70 \text{ km} ,$$

x (solar activity, SSN) = 0 for low sunspot number (used here); otherwise not clear in Reference 8.

where

SSN = smoothed Zurich sunspot number

$$x\ (\text{season}) = \cos \left(\frac{m - 0.5}{12} 2\pi \right)$$

where

m = month, and

x (magnetic index) = 0, quiet conditions
= 1, disturbed conditions.

Tables 6 and 7 show the constants generated by McNamara to fit over 700 profiles, and Figures 2 and 3 show the electron concentration profiles for mid-latitude, magnetically-quiet conditions. Winter and summer conditions are plotted for two-hour intervals from midnight to noon. Selected reference exponential profiles ($\beta = 0.7$, $h_w = 88$ for night and $\beta = 0.3$, $h_w = 72$ for day)

Table 6. The coefficients of the regression equation at heights from 55 to 90 km for magnetically quiet days (from Reference 8).

Height (km)	Constant	Zenith Angle	Latitude	Solar Activity	Season
90	3.21	0.80	0	0	0.15
85	2.32	0.86	0.23	0.13	0.16
80	1.87	1.03	0.16	0.20	0.17
75	1.64	1.00	0.09	0.25	0
70	1.49	0.86	0.17	0.13	-0.05
65	1.25	0.57	0.58	0.26	0
60	0.81	0.66	0.78	0.26	0.12
55	0.82	0.77	0	0	0

Table 7. The coefficients of the regression equation at heights from 55 to 90 km for all magnetic conditions (from Reference 8).

Height (km)	Constant	Zenith Angle	Latitude	Solar Activity	Season	Magnetic Effect Term
90	3.12	0.82	0	0.15	0.17	0.17
85	2.30	0.86	0.24	0.15	0.18	0.34
80	1.88	0.98	0.15	0.22	0.18	0.31
75	1.66	0.95	0.09	0.26	0	0.32
70	1.49	0.84	0.18	0.13	-0.06	0.32
65	1.25	0.58	0.57	0.26	0	0.21
60	0.81	0.68	0.78	0.25	0.12	0.45
55	0.82	0.77	0	0	0	0

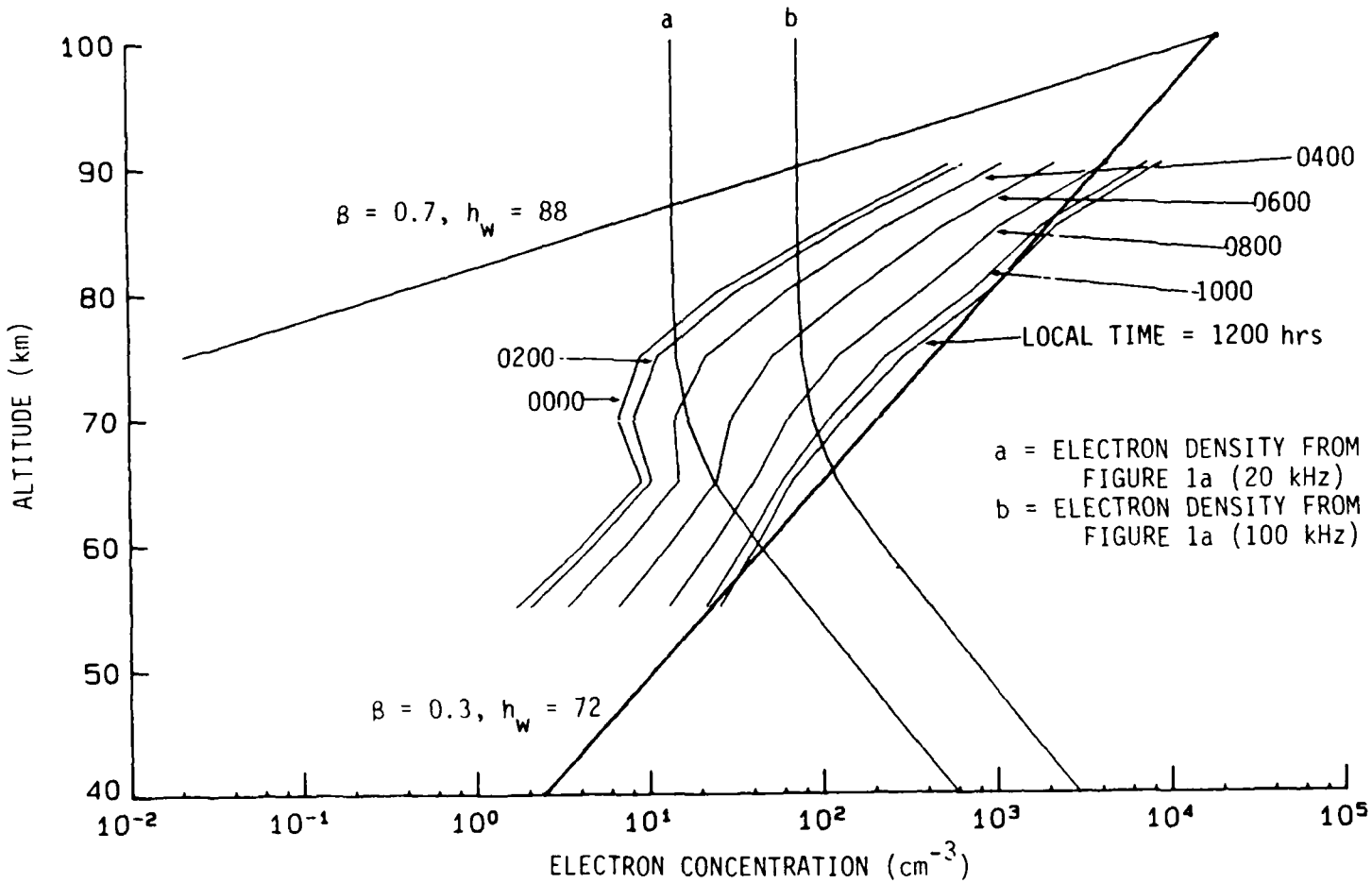

Figure 2. Electron concentration from McNamara's model (summer, magnetically quiet, low sunspot number, midlatitude conditions).

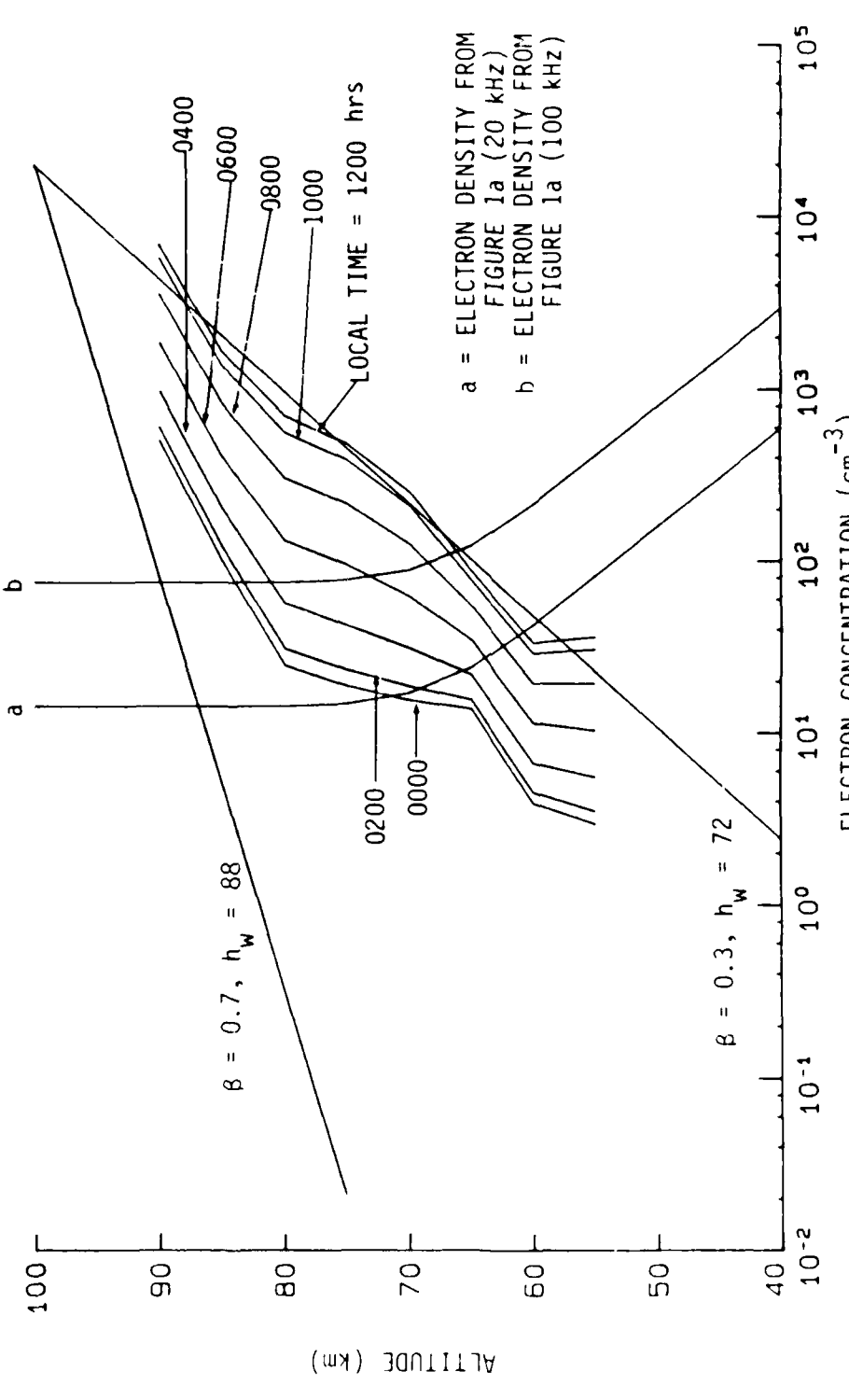

Figure 3. Electron concentration from McNamara's model (winter, magnetically quiet, low sunspot number, midlatitude conditions).

are also shown. It can be seen that the model agrees reasonably well with the daytime exponential, but produces electron concentrations significantly larger than the nighttime exponential.

2.3 PHYSICAL MODELS.

2.3.1 WECOM Models.

Physical models of D-region ionization for use in weapon effects prediction have been developed by Knapp (References 9 and 10) and Knapp and Jordano (Reference 11) and these models are regularly updated. The models incorporate results of very complex simulations of D-region chemistry and also tune results to match observed nuclear produced effects. Unfortunately the useful nuclear data are absorption data, are pertinent to medium to strong disturbance conditions, and provide little help in defining models for weak VLF/LF disturbance or recovery predictions. The models include a complex mixture of atomic and molecular species and associated reactions. In the model reactions between different species are combined for specific conditions to produce effective lumped-parameter reaction rate coefficients. The lumped-parameter coefficients are:

A = attachment rate s^{-1}

D = detachment rate s^{-1}

α_i = ion-ion recombination coefficient $cm^3\ s^{-1}$

α_D = ion-electron recombination coefficient $cm^3\ s^{-1}$.

These parameters are used in transient equations (Equations 11 through 14) and in quasi-equilibrium equations (Equations 15 through 17).

$$\frac{dN_e}{dt} = q - \alpha_d N_e N_+ - AN_e + DN_- \qquad (11)$$

$$\frac{dN_-}{dt} = -\alpha_i N_- N_+ + AN_e - DN_- \qquad (12)$$

$$\frac{dN_+}{dt} = q - \alpha_i N_- N_+ - \alpha_d N_e N_+ \qquad (13)$$

$$N_+ = N_e + N_- \qquad (14)$$

where

q = ion production rate $cm^{-3}\ s^{-1}$.

$$N_+ = \sqrt{\frac{q}{\alpha}} \tag{15}$$

$$\alpha = \frac{A\alpha_i + D\alpha_D + \alpha_i\alpha_D\sqrt{\frac{q(A+D)}{A\alpha_i + D\alpha_D}}}{A + D + \alpha_i\sqrt{\frac{q(A+D)}{A\alpha_i + D\alpha_D}}} \tag{16}$$

$$N_e = \frac{q + D\sqrt{\frac{q}{\alpha}}}{A + D + \alpha_D\sqrt{\frac{q}{\alpha}}} \quad . \tag{17}$$

Equation 16 is solved iteratively for α .

For normal ionosphere models, we will usually be interested in quasi-equilibrium solutions, although the limitation imposed by the transient equations on the decay from daytime profiles to desired nighttime profiles will be discussed.

Knapp (Reference 9) improved the VLF/LF predictions of the WEDCOM code (Reference 2) by incorporating the Berry model into the physical model. This was done by forcing the physical model to reproduce Berry's results over the altitude range

$$h_r \pm \frac{1}{\beta} \quad .$$

The force-fitting is done by adjusting the normal ion production rates to produce Berry's results. Berry's model results and the WEDCOM chemistry model results are sufficiently close together for most cases that this adjustment can be made while retaining reasonable values of ion production rates. In the WEDCOM code, only noon and midnight profiles are used.

More recently, the D-region model has been combined with a time-varying E- and F-region model used for HF. Knapp (Reference 9) has adjusted the model to merge smoothly into the empirical E-region model ionosphere. This is also done by adjusting normal production rates to include an effective q to match E-region electron densities above 90 km.

Figures 4 and 5 show electron concentration produced by the WECOM model as a function of altitude and parametric in time (two-hour periods) for mid-latitude summer and winter conditions. Tables 8 and 9 show the corresponding reaction rates for midnight and noon conditions. The exponential region (straight-line portion of the figures) that results from forcing Berry's results can be seen in the figures and, for the most part the transition points are reasonable.

As was the case for Berry's results, the nighttime electron concentrations are significantly higher in the 75 to 85 km altitude range than the hypothetical profile values used to match propagation data. Figures 6 and 7 show only the midnight and noon profiles from the WECOM model. Also shown on the figures are selected reference exponential profiles that have been found to reproduce some VLF and LF propagation data. A replot of Figure 1a, to emphasize the important reflecting region of the profiles is also shown on the figures. Note that the daytime profile and the proposed exponential profile are nearly equal in the reflecting range. The nighttime WECOM profile will produce reflection at significantly lower altitudes than the exponential profile and the irregularity at 75 and 85 km will have some effect on propagation predictions. Some possible adjustments to the physical model to produce a closer match to the nighttime exponentials are discussed in Section 3.

2.3.2 SIMBAL Models.

The SIMBAL code (Reference 1) includes a D-region model that was developed using an earlier (1981) version of D-region models used in weapon effects codes (then called WEPH VI, References 12 and 13). The procedure used was to compute $N_e(h)$ and $N_+(h)$ as a function of ion production $Q(h)$, with $Q(h)$ varying from normal to about 10^{10} × normal. The electron and ion profiles were fit with equations of the form

$$N_e = \exp\left(C_e + x \ln Q\right) \tag{18}$$

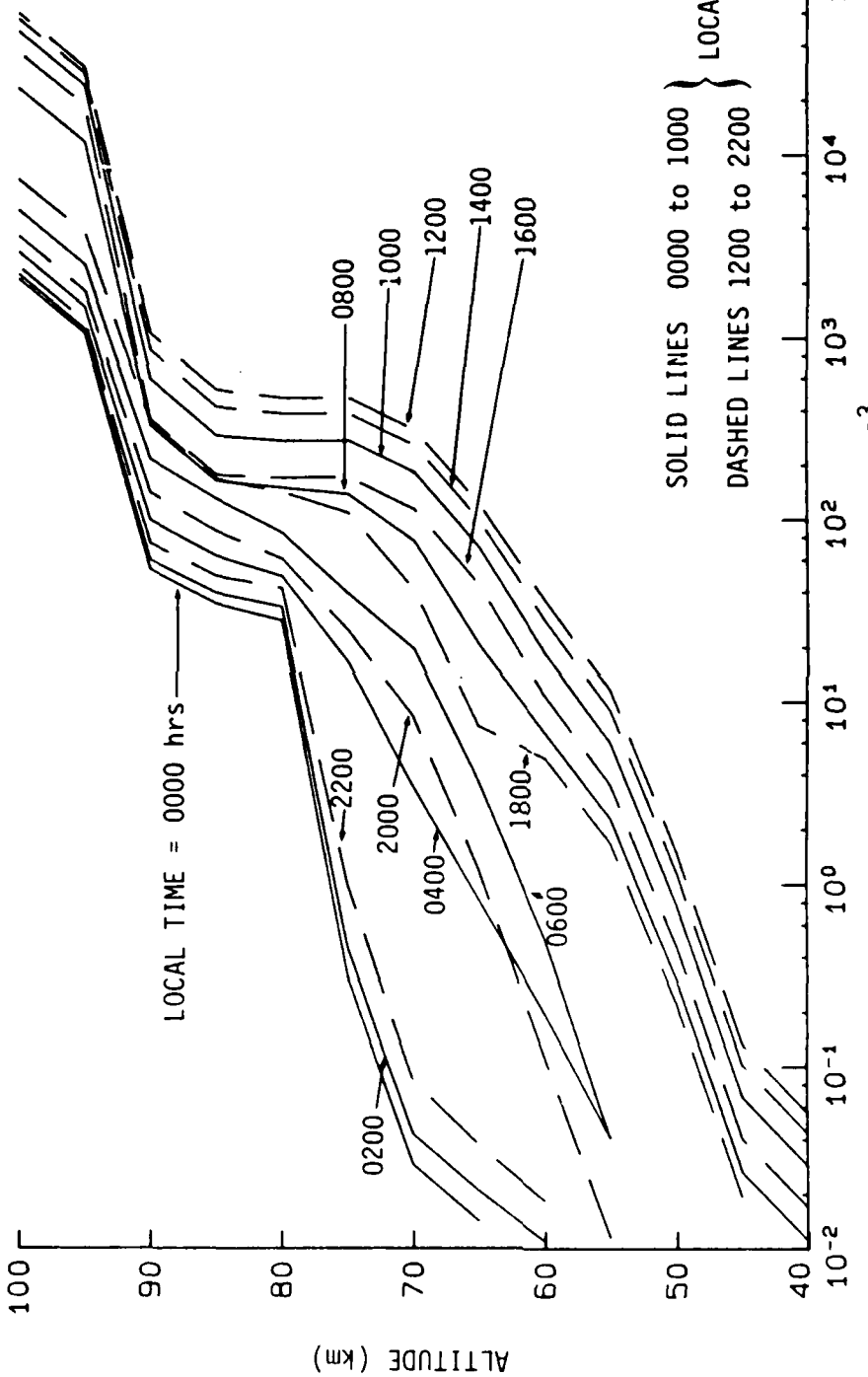

Figure 4. WECOM model electron concentration profiles for winter, 40 degrees latitude, SSN = 80.

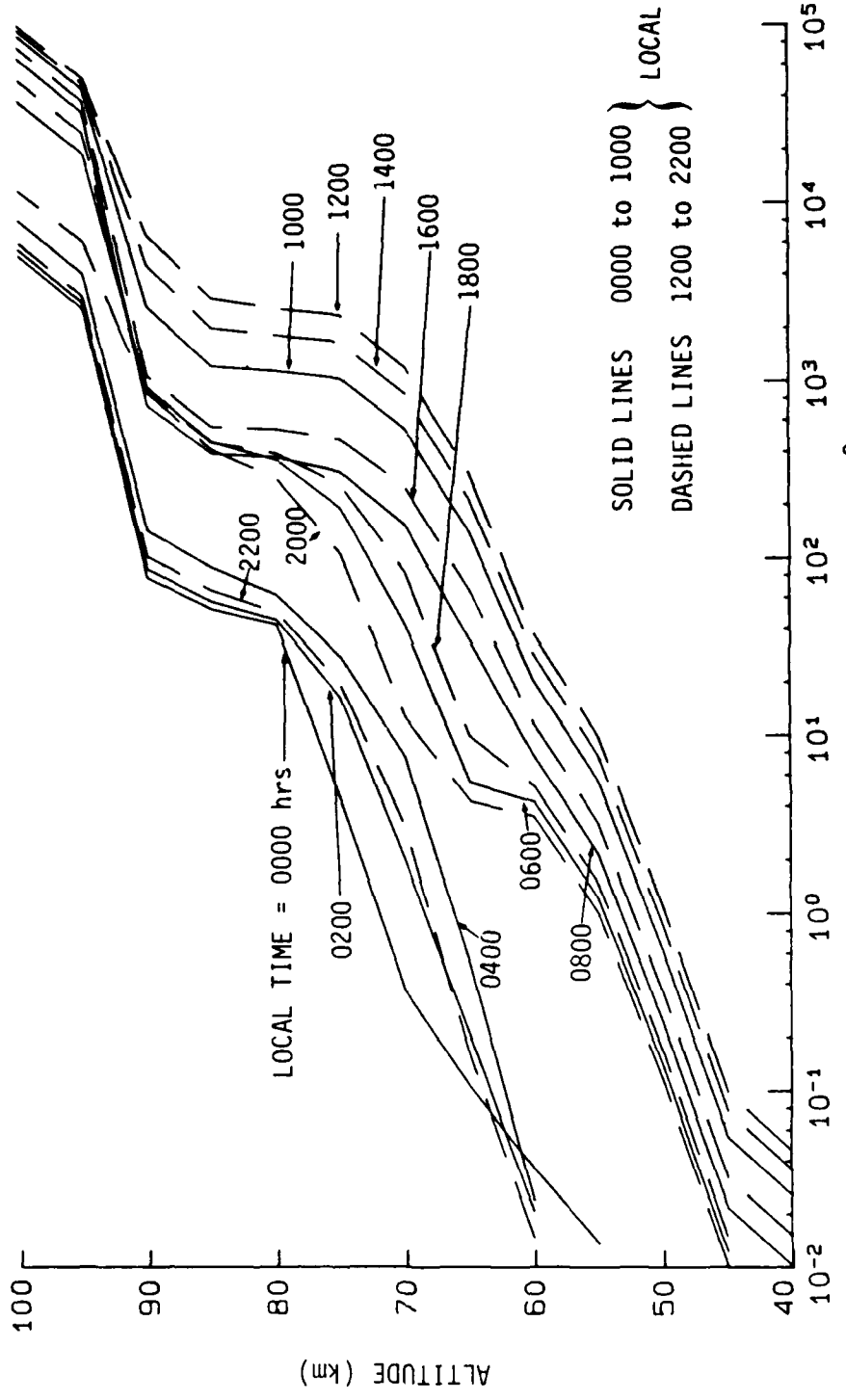

Figure 5. WECOM model electron concentration profiles for summer, 40 degrees latitude, SSN = 100.

Table 8. WECOM reaction rates for midlatitude winter conditions.

MIDNIGHT

Height (km)	α_i	α_D	D	A	Q_a
0.	3.20E-06	5.17E-06	9.67E-10	7.85E+07	2.86E-01
5.	2.36E-06	5.40E-06	5.29E-11	2.03E+07	2.91E+00
10.	1.75E-06	5.72E-06	5.56E-12	5.29E+06	8.17E+00
15.	1.02E-06	5.87E-06	1.98E-12	1.16E+06	9.25E+00
20.	5.06E-07	5.85E-06	2.17E-12	2.37E+05	6.09E+00
25.	2.56E-07	5.62E-06	3.86E-12	4.83E+04	3.06E+00
30.	1.49E-07	5.06E-06	7.35E-12	1.02E+04	1.32E+00
35.	9.99E-08	4.25E-06	2.72E-11	2.22E+03	6.18E-01
40.	7.90E-08	3.95E-06	1.24E-10	5.19E+02	2.93E-01
45.	6.99E-08	3.62E-06	4.72E-10	1.31E+02	1.44E-01
50.	6.62E-08	3.22E-06	1.01E-09	3.62E+01	7.50E-02
55.	6.58E-08	3.16E-06	8.04E-10	1.04E+01	4.09E-02
60.	6.64E-08	3.26E-06	3.00E-10	2.97E+00	2.22E-02
65.	6.77E-08	3.49E-06	7.33E-11	8.35E-01	1.19E-02
70.	6.93E-08	3.72E-06	1.26E-10	2.14E-01	6.27E-03
75.	7.12E-08	3.80E-06	5.76E-05	4.72E-02	3.23E-03
80.	7.32E-08	2.32E-06	1.93E-02	9.49E-03	2.78E-03
85.	7.45E-08	2.24E-06	2.39E-02	3.93E-03	3.15E-03
90.	7.42E-08	1.66E-06	2.16E-02	1.33E-03	4.94E-03
95.	7.24E-08	5.87E-07	4.15E-01	7.40E-04	6.57E-01
100.	7.04E-08	5.31E-07	1.60E+00	7.97E-04	2.35E+00

NOONTIME

Height (km)	α_i	α_D	D	A	Q_a
0.	3.20E-06	5.17E-06	2.98E-02	7.85E+07	1.39E-01
5.	2.36E-06	5.40E-06	2.94E-02	2.03E+07	1.41E+00
10.	1.75E-06	5.72E-06	2.73E-02	5.29E+06	3.97E+00
15.	1.02E-06	5.87E-06	2.70E-02	1.16E+06	4.49E+00
20.	5.06E-07	5.85E-06	2.77E-02	2.37E+05	2.96E+00
25.	2.56E-07	5.62E-06	2.82E-02	4.83E+04	1.49E+00
30.	1.49E-07	5.06E-06	2.83E-02	1.02E+04	6.41E-01
35.	9.99E-08	4.25E-06	2.68E-02	2.22E+03	3.00E-01
40.	7.90E-08	3.95E-06	2.14E-02	5.19E+02	1.42E-01
45.	6.99E-08	3.62E-06	1.73E-02	1.31E+02	7.00E-02
50.	6.62E-08	3.23E-06	7.75E-02	3.61E+01	3.63E-02
55.	6.58E-08	3.09E-06	3.66E-01	1.04E+01	1.97E-02
60.	6.64E-08	3.01E-06	1.63E+00	2.92E+00	1.14E-02
65.	6.77E-08	3.02E-06	3.84E+00	7.78E-01	5.34E-02
70.	6.93E-08	2.74E-06	5.30E+00	1.93E-01	2.78E-01
75.	7.12E-08	2.15E-06	7.74E+00	4.42E-02	4.75E-01
80.	7.32E-08	2.02E-06	1.23E+01	9.49E-03	4.42E-01
85.	7.45E-08	1.65E-06	2.06E+01	2.35E-03	4.42E-01
90.	7.42E-08	7.97E-07	3.56E+01	6.80E-04	8.79E-01
95.	7.24E-08	4.70E-07	8.39E+01	6.20E-04	4.32E+02
100.	7.04E-08	4.41E-07	1.17E+02	7.83E-04	1.56E+03

Table 9. WECOM reaction rates for midlatitude summer conditions.

MIDNIGHT

Height (km)	α_i	α_D	D	A	Q_a
0.	2.58E-06	5.00E-06	3.29E-08	8.81E+07	7.24E-01
5.	2.06E-06	5.27E-06	4.70E-10	2.12E+07	5.99E+00
10.	1.66E-06	5.62E-06	1.88E-11	5.89E+06	1.74E+01
15.	1.09E-06	5.88E-06	2.94E-12	1.36E+06	2.17E+01
20.	5.18E-07	5.77E-06	4.77E-12	2.76E+05	1.46E+01
25.	2.54E-07	5.26E-06	1.24E-11	5.77E+04	7.57E+00
30.	1.45E-07	4.45E-06	3.38E-11	1.27E+04	3.39E+00
35.	9.86E-08	4.04E-06	1.22E-10	2.95E+03	1.69E+00
40.	7.87E-08	3.82E-06	4.48E-10	7.33E+02	8.90E-01
45.	6.96E-08	3.45E-06	1.49E-09	1.95E+02	5.05E-01
50.	6.59E-08	3.03E-06	3.24E-09	5.54E+01	3.19E-01
55.	6.54E-08	2.96E-06	2.80E-09	1.65E+01	2.26E-01
60.	6.61E-08	3.09E-06	1.17E-09	4.82E+00	1.74E-01
65.	6.80E-08	3.55E-06	3.45E-10	1.38E+00	1.45E-01
70.	7.08E-08	4.09E-06	1.03E-09	3.48E-01	1.28E-01
75.	7.41E-08	4.32E-06	1.89E-04	7.21E-02	1.19E-01
80.	7.81E-08	3.34E-06	3.59E-02	1.25E-02	8.12E-03
85.	8.15E-08	2.75E-06	3.45E-02	3.65E-03	8.14E-03
90.	7.93E-08	2.39E-06	2.70E-02	1.07E-03	1.52E-02
95.	7.72E-08	6.45E-07	8.57E-01	5.95E-04	4.26E+00
100.	7.48E-08	5.66E-07	3.04E+00	6.01E-04	1.47E+01

NOONTIME

Height (km)	α_i	α_D	D	A	Q_a
0.	2.58E-06	5.00E-06	2.98E-02	8.81E+07	1.45E-01
5.	2.06E-06	5.27E-06	2.94E-02	2.12E+07	1.38E+00
10.	1.66E-06	5.62E-06	2.73E-02	5.89E+06	4.08E+00
15.	1.09E-06	5.88E-06	2.70E-02	1.36E+06	5.08E+00
20.	5.18E-07	5.77E-06	2.77E-02	2.76E+05	3.42E+00
25.	2.54E-07	5.26E-06	2.82E-02	5.77E+04	1.75E+00
30.	1.45E-07	4.45E-06	2.83E-02	1.27E+04	7.71E-01
35.	9.86E-08	4.04E-06	2.69E-02	2.95E+03	3.72E-01
40.	7.87E-08	3.82E-06	2.19E-02	7.33E+02	1.83E-01
45.	6.96E-08	3.45E-06	1.64E-02	1.95E+02	9.30E-02
50.	6.59E-08	3.08E-06	7.22E-02	5.53E+01	4.92E-02
55.	6.54E-08	2.94E-06	3.53E-01	1.65E+01	2.72E-02
60.	6.61E-08	2.91E-06	1.67E+00	4.77E+00	1.64E-02
65.	6.80E-08	3.16E-06	4.19E+00	1.31E+00	3.70E-01
70.	7.08E-08	3.12E-06	6.23E+00	3.22E-01	4.75E+00
75.	7.41E-08	2.25E-06	9.69E+00	6.87E-02	1.26E+01
80.	7.81E-08	2.12E-06	1.53E+01	1.25E-02	1.43E+01
85.	8.15E-08	1.78E-06	2.34E+01	2.29E-03	1.53E+01
90.	7.93E-08	6.83E-07	3.44E+01	5.63E-04	3.01E+01
95.	7.72E-08	4.45E-07	7.14E+01	5.11E-04	1.15E+03
100.	7.48E-08	4.13E-07	8.87E+01	5.93E-04	4.06E+03

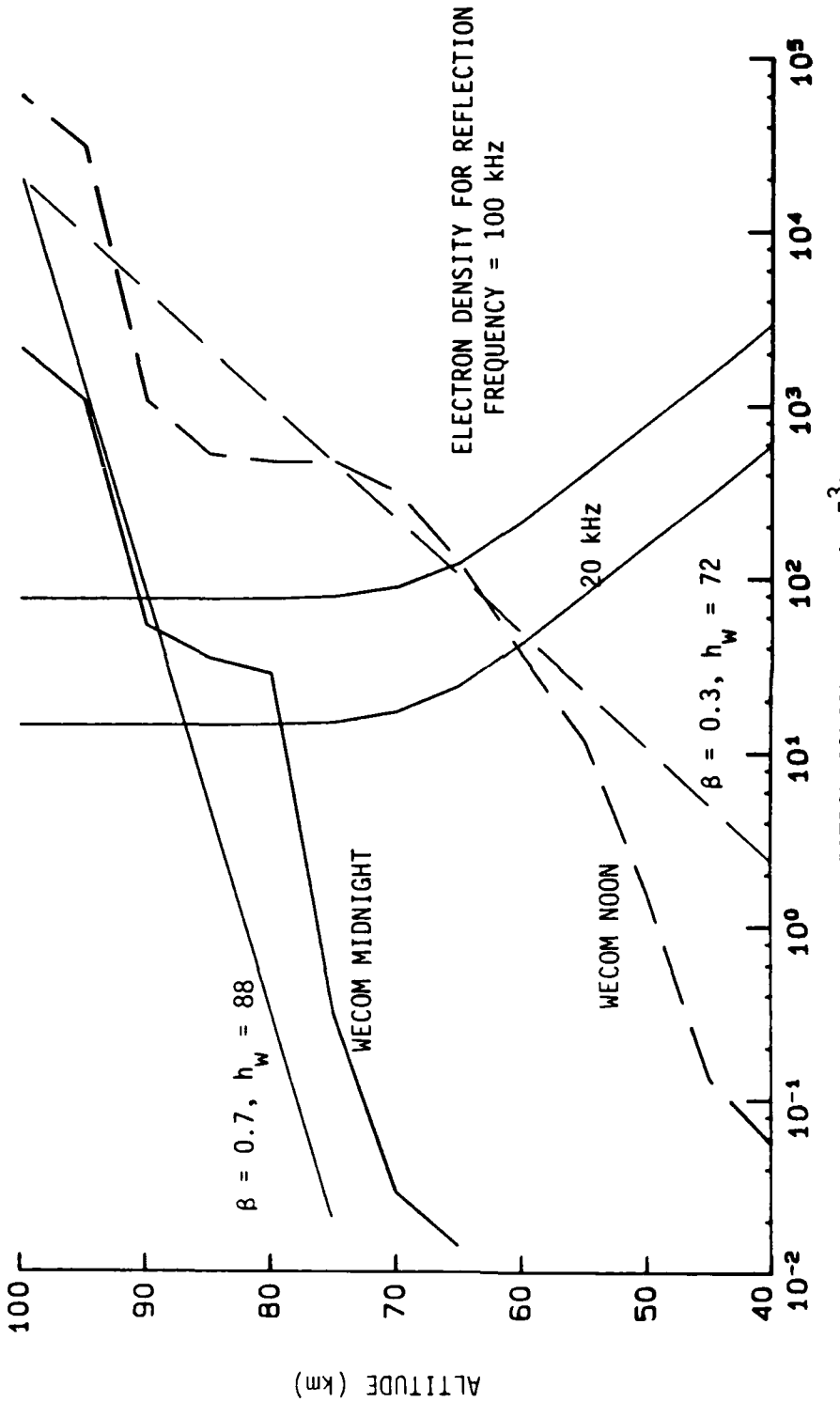

Figure 6. WECOM noon and midnight profiles compared to widely used exponential profiles for winter, 40 degrees latitude, SSN = 80.

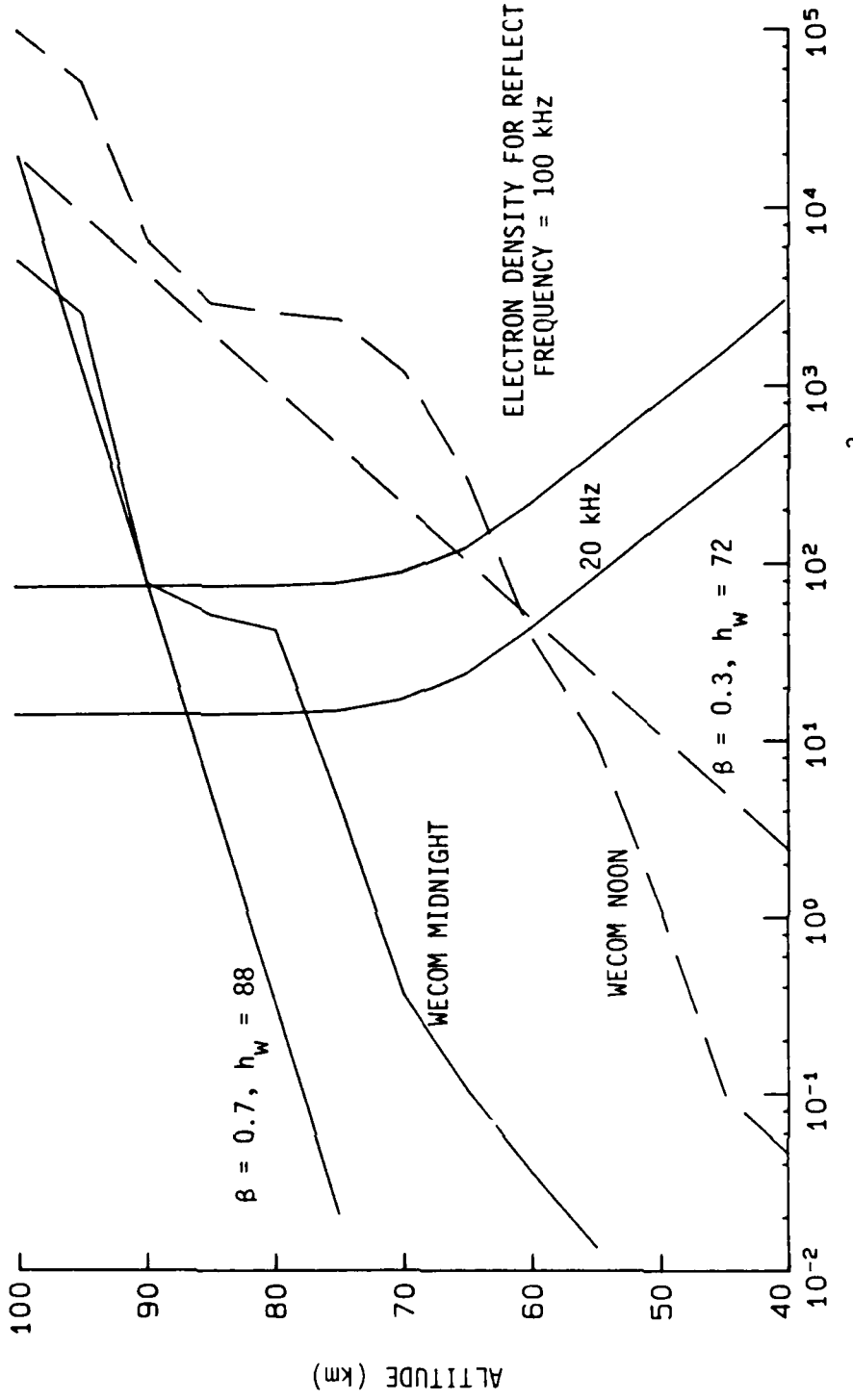

Figure 7. WECOM noon and midnight profiles compared to widely used exponential profiles for summer, 40 degrees latitude, SSN = 100.

$$N_+ = \exp\left(C_+ + y \ln Q\right) \tag{19}$$

where there are one or two sets of C_e's, C_+'s, x's, and y's for each altitude. Two sets are required - one set for large Q , one set for small Q at some altitudes. Equations 18 and 19 are more efficient than the quasi-equilibrium equations. They also have the advantage of including the dependence of the lumped-parameter reaction rates on production rate.

Figure 8 shows SIMBAL normal electron density concentration compared to selected exponential profiles. In the SIMBAL program only day (noon) and night (midnight) profiles are used. Transition across the day-night terminator is abrupt. Comparison of Figure 8 with Figures 6 and 7 shows that the SIMBAL daytime model is relatively consistent with the newer WECOM model and the SIMBAL normal nighttime model is intermediate between the summer and winter nighttime values for WECOM.

The nighttime VLF loss rates estimated using the SIMBAL nighttime profiles are higher than most observed values and this discrepancy has resulted in requests by SIMBAL code users to define a revised model that would produce predictions which agree better with observed losses. Some comparisons between SIMBAL and measured data are shown in Figures 9 through 12. The SIMBAL program, which is normally used to compute propagation effects between two fixed locations, uses a RMS mode or hop sum instead of a vector sum, to avoid sensitivity to predicting the location of peaks and nulls. The RMS sum results in a smooth variation in field strength versus distance. The SIMBAL field strengths have, in general, the correct magnitude for daytime conditions, but are generally lower than measured values for nighttime conditions.

Results are also shown from the VLFSIM program (Reference 14), which uses the RMS summing technique similar to SIMBAL, but the undisturbed ionosphere model has been modified to use precomputed mode constants for the $\beta = 0.7$, $h_w = 88$ km profile. Predictions using VLFSIM show generally better agreement with measured data for nighttime conditions than the SIMBAL results.

The technique used to force the VLFSIM ionosphere model to relax to the exponential profile for no disturbance is discussed in Section 3.

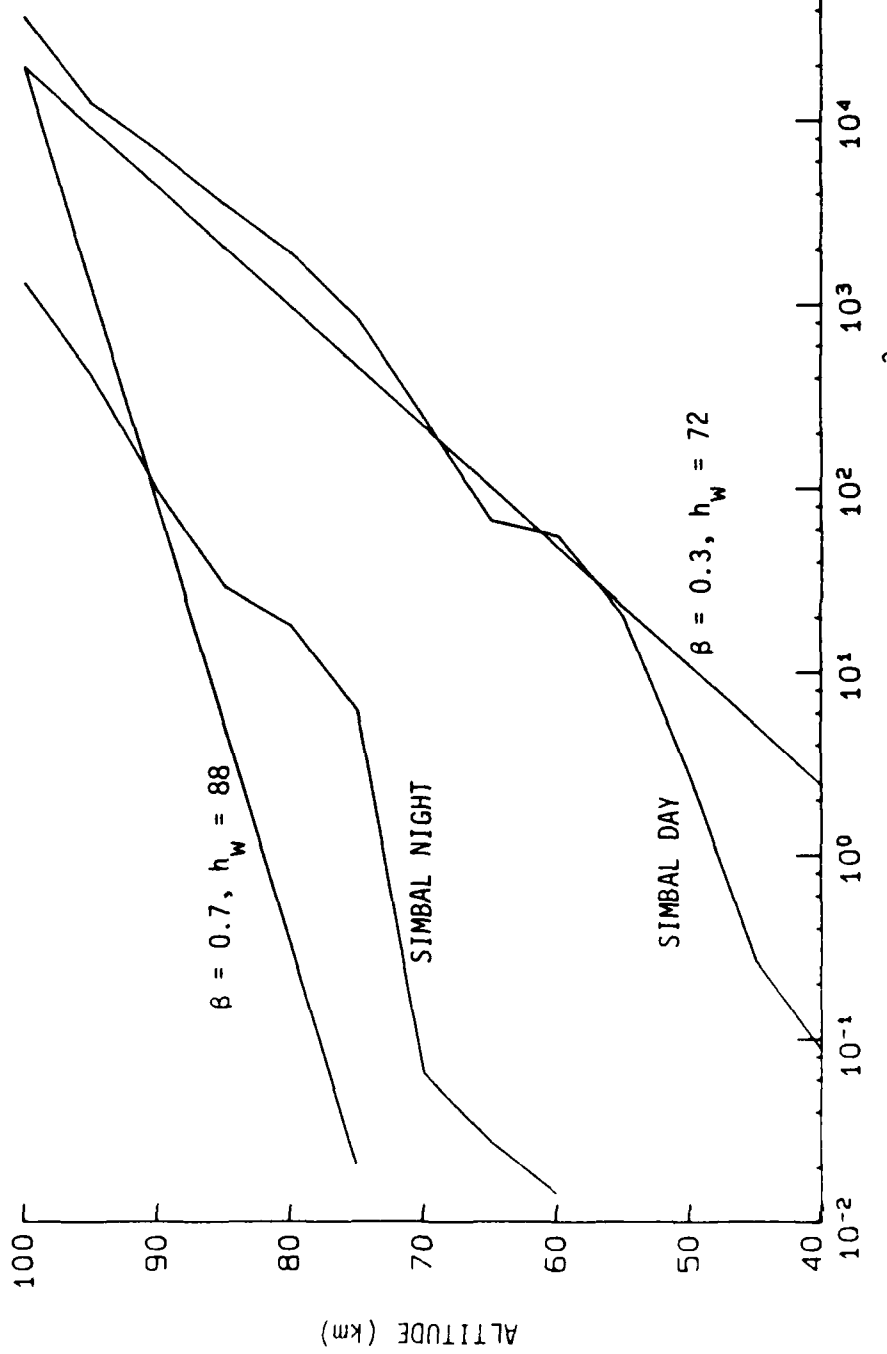

Figure 8. SIMBAL day and night profiles compared to widely used exponential profiles.

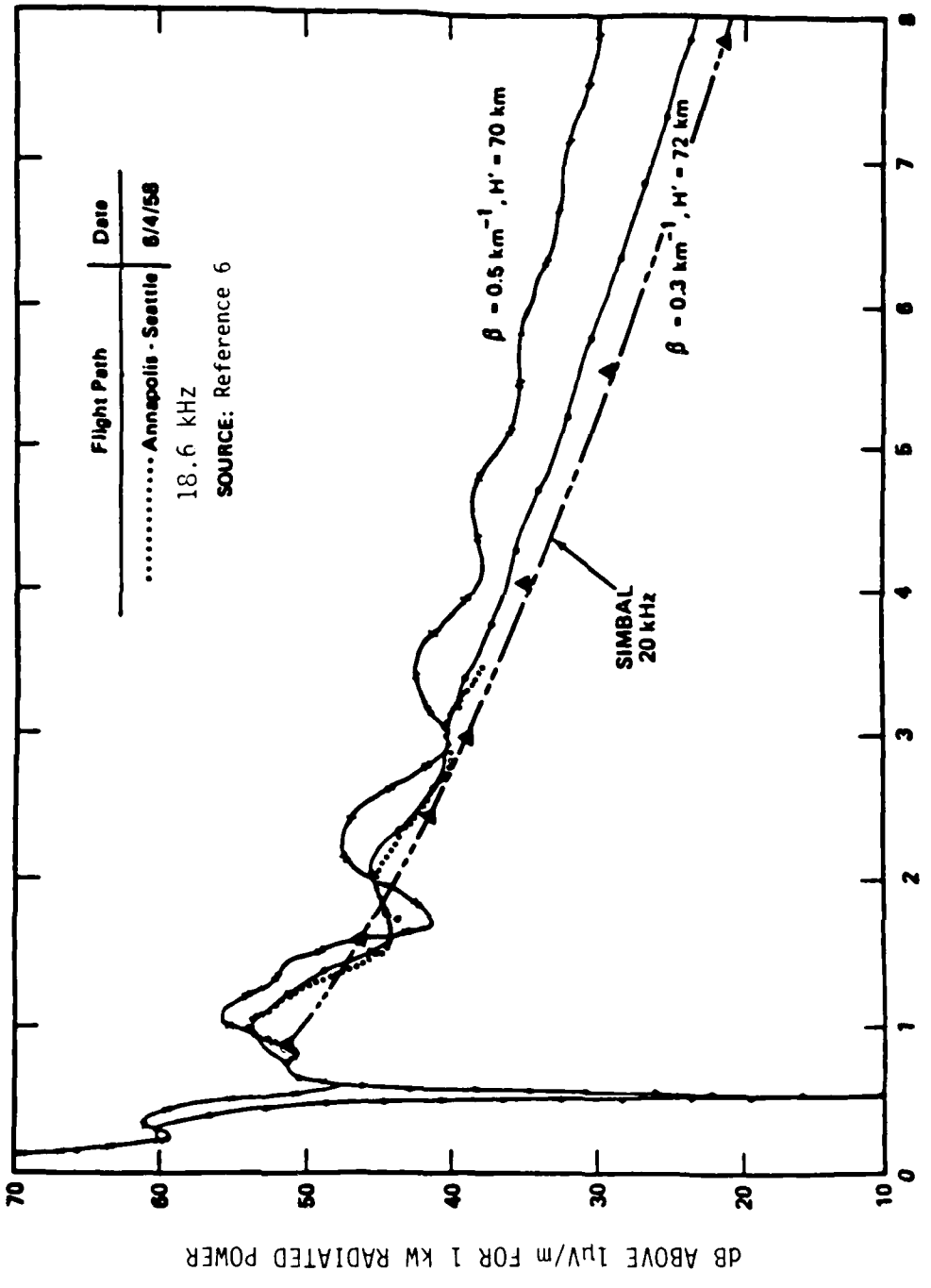

Figure 9. Comparison of SIMBAL 20 kHz daytime predictions with data and calculations from Reference 6.

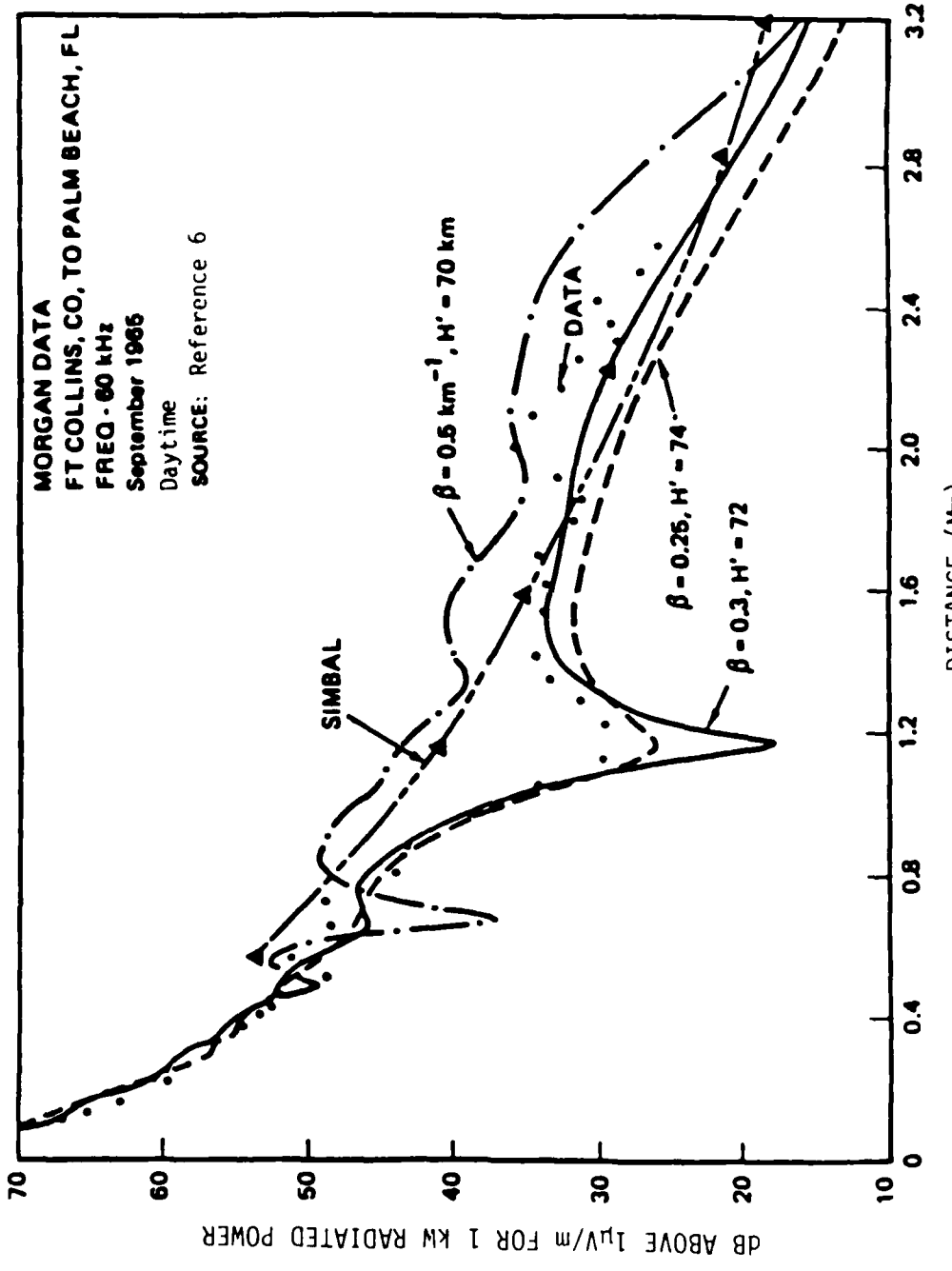

Figure 10. Comparison of SIMBAL 60 kHz daytime predictions with data and calculations from Reference 6.

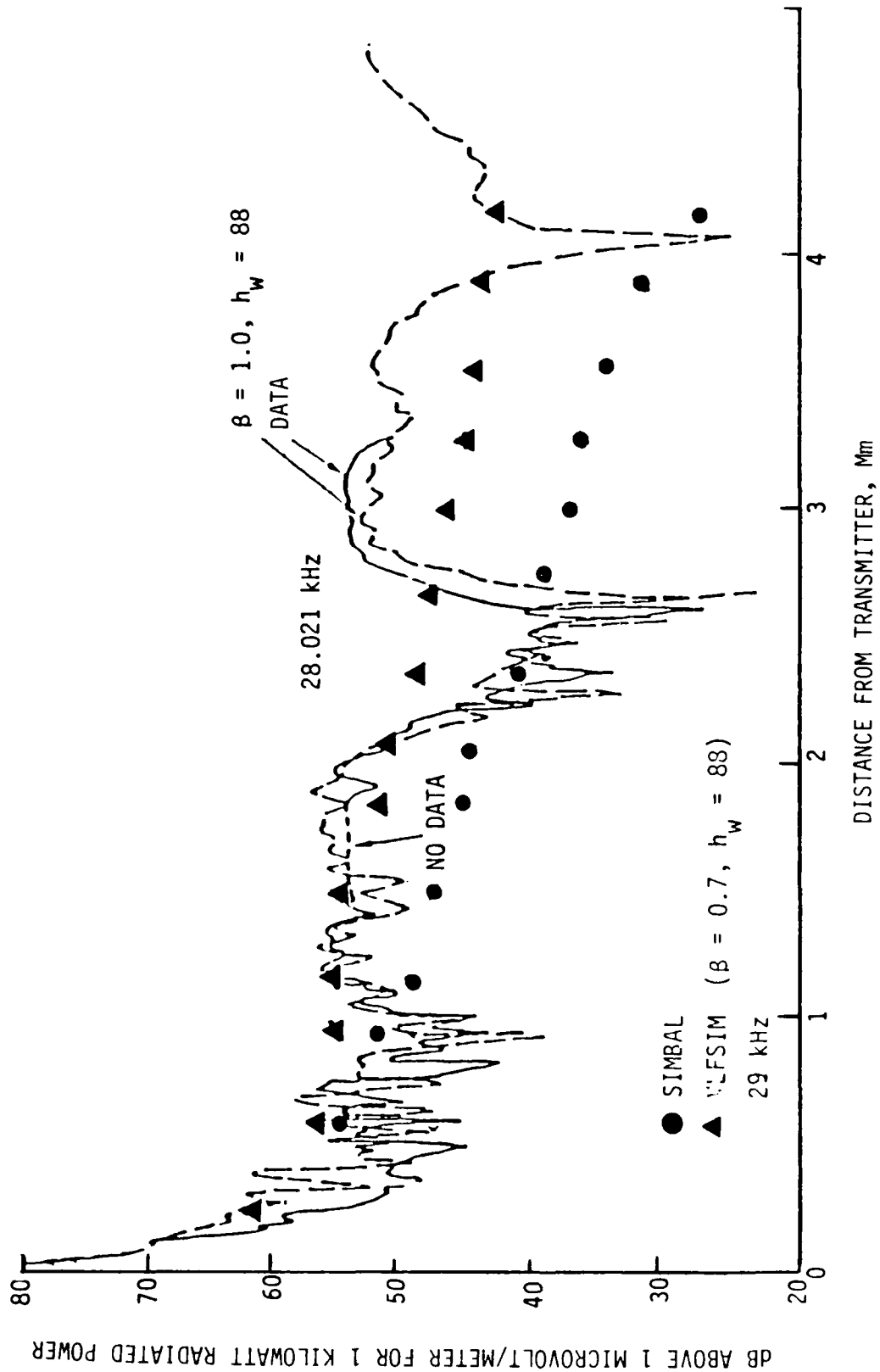

Figure 11. Comparison of SIMBAL and VLFSIM 29 kHz nighttime predictions with data and calculations from Reference 6.

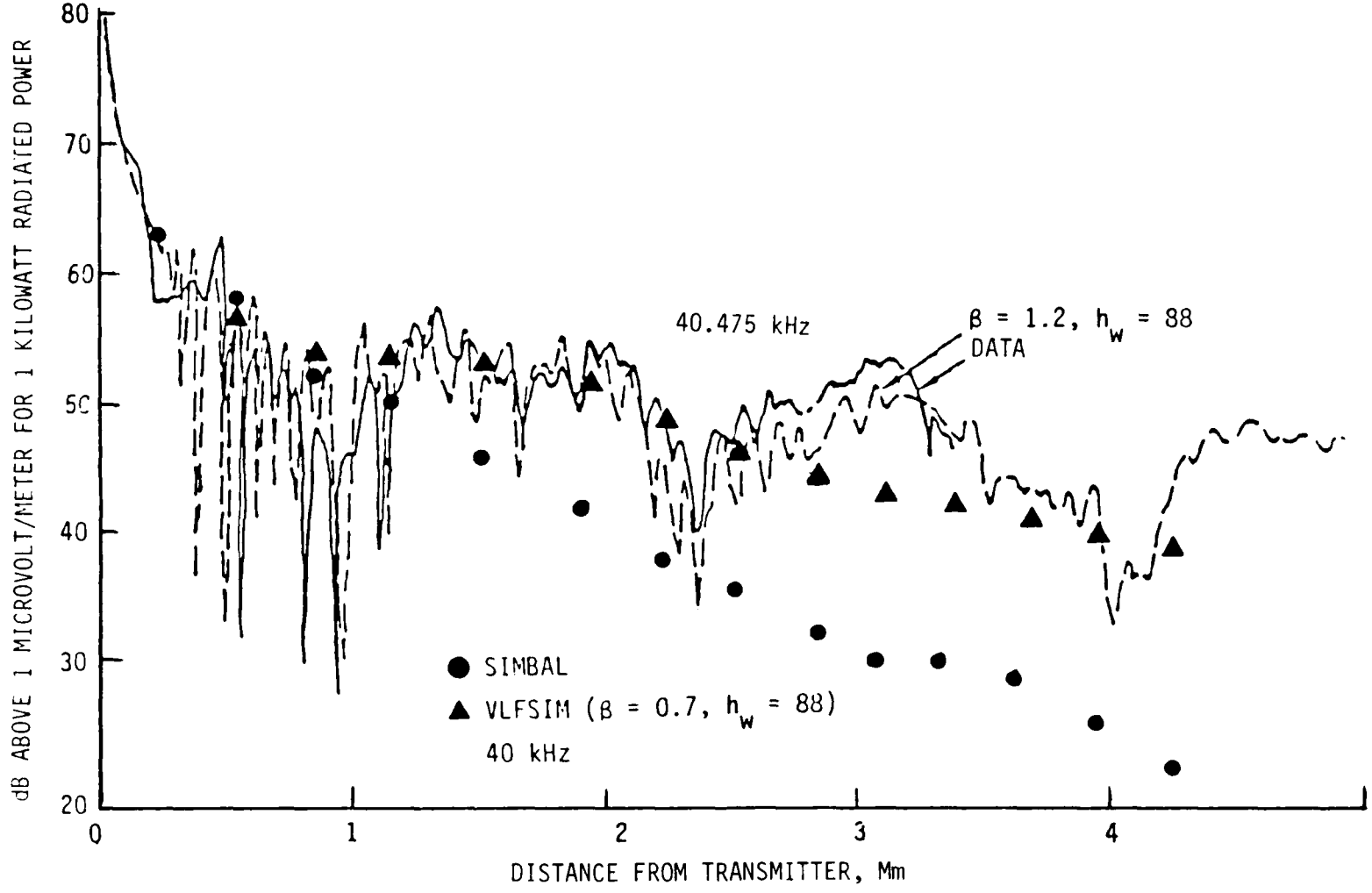

Figure 12. Comparison of SIMBAL and VLFSIM 40 kHz nighttime predictions with data and calculations from Reference 6.

2.4 PROFILES TO MATCH HF ABSORPTION PREDICTIONS.

HF D-region absorption is predicted by integrating the absorption through the D and lower E region or by using empirical models that estimate absorption directly. The most recent CCIR approved model is used in IONCAP (Reference 15) and computes the absorption per semi-hop using

$$A\ (dB) = \frac{338\ I\ \sec\ \phi}{\left(f + f_H\right)^{1.98} + 10.2} \tag{20}$$

where

f = wave frequency (MHz)

f_H = longitudinal component of the gyrofrequency (MHz)

ϕ = angle of incidence of the ray at the D region.

$$I = -0.04 + \exp\ (-2.937 + 0.8445\ f_{oE}) \tag{21}$$

where

f_{oE} = E-layer critical frequency.

The WECOM model is compared to the empirical predictions by integrating vertical one-way absorption through the D-region profiles shown in Figures 4 and 5 and comparing to results produced using Equations 20 and 21. The profiles and the E-layer critical frequency were both computed using an analytic model (Reference 16) for the E-region parameters. The values obtained for a frequency of 10 MHz are shown in Table 10.

The integral and empirical values agree reasonably well near summer noon, but are about a factor of 2 low for other times (when absorption is important). An increase in electron density above about 70 km for daytime conditions would improve the agreement between the two models and have little affect on VLF/LF propagation predictions.

HF absorption data and associated models provide no useful information to deduce nighttime profiles for VLF/LF propagation.

Table 10. One-way vertical absorption at 10 MHz, latitude = 40 degrees, SSN = 100.

	Summer			Winter		
Local Time (hr)	FOE (MHz)	Empirical (dB)	Integral (dB)	FOE (MHz)	Empirical (dB)	Integral (dB)
0	0.787	0.17	3.48^{-2}	0.52	0.12	2.31^{-2}
2	0.816	0.18	4.57^{-2}	0.54	0.12	2.50^{-2}
4	0.989	0.23	6.39^{-2}	0.62	0.13	4.10^{-2}
6	2.21	0.83	0.38	0.81	0.18	6.57^{-2}
8	3.00	1.72	0.58	1.80	0.55	0.32
10	3.54	2.79	1.46	2.67	1.28	0.70
12	3.78	3.44	2.68	3.01	1.74	1.03
14	3.68	3.15	2.04	2.89	1.56	0.90
16	3.26	2.17	0.883	2.31	0.91	0.50
18	2.58	1.17	0.497	0.99	0.22	0.15
20	1.20	0.29	0.147	0.69	0.15	4.10^{-2}
22	0.865	0.19	4.62^{-2}	0.57	0.12	2.00^{-2}

SECTION 3
ADJUSTING PROFILES TO MATCH PROPAGATION DATA

3.1 GENERAL.

The previous sections have provided some comparisons between D-region electron concentration profiles produced by selected D-region ionosphere models and profiles inferred from comparisons between measured and predicted VLF and LF propagation data. The differences between model profiles and profiles required to match data are not great for daytime conditions, but are frequently large for nighttime conditions. In general, the propagation predictions require a lower electron concentration in the altitude range from 75 to 95 km than the models produce.

A coordinated program to simultaneously collect electron concentration measurements and propagation measurements over a period of time would be required to completely resolve model differences. However, *VLF and LF propagation* parameters do provide a sensitive measure of low-concentration profile properties, and there is good reason to have model predictions reproduce measured data in the undisturbed case as a starting or recovery point for nuclear disturbed predictions.

Two model parameters (ion production rate and atmospheric chemistry reaction rates) can be adjusted separately or jointly to force model profiles to take on prescribed values. The method chosen to make the adjustment should use values that are within the bounds of uncertainty of the parameters. Also, as will be shown later, the effects of adjusting the two sets of parameters are sometimes coupled and must be considered jointly.

Reducing the normal ion production rate to reduce electron density to match selected profiles will result in increasing the sensitivity to low levels of weapon ionization. On the other hand, modifying the chemistry to decrease electron density will decrease the sensitivity to low level disturbances.

In the following subsections, the altitude region where profile matching is required, and procedures for matching specified profiles are addressed.

3.2 ALTITUDE REGIONS FOR MATCHING.

Equations 2 and 3 can be used to define altitudes where VLF reflection maximizes. Detailed calculations of ionospheric reflection coefficients from two selected exponential profiles were performed to estimate the altitude range over which a smooth exponential variation must be maintained to provide answers nearly the same as obtained when the exponential profile is assumed for all altitudes. The profiles examined were selected to be (β = 0.3, h_w = 72) for daytime and (β = 0.7, h_w = 88) for nighttime. The calculations tested to define upper and lower altitudes where a change of slope could be introduced without changing the reflection coefficient values.

The actual profiles used in the analysis were:

$$N_e(h) = N_o \exp(-0.7 \times 88) \exp(0.55\, h), \qquad h_\ell < h < h_u$$

$$N_e(h) = N_e(h_\ell) \exp(0.35\,(h - h_\ell)) \qquad h < h_\ell$$

$$N_e(h) = N_e(h_u) \exp(0.35\,(h - h_u)) \qquad h > h_u$$

for nighttime and

$$N_e(h) = N_o \exp(-0.3 \times 72) \exp(0.15\, h), \qquad h_\ell < h < h_u$$

$$N_e(h) = N_e(h_\ell) \exp(0.3\,(h - h_\ell)) \qquad h < h_\ell$$

$$N_e(h) = N_e(h_u) \exp(0.3\,(h - h_u)) \qquad h > h_u$$

for daytime conditions where

$$N_o = 1.43 \times 10^7 \text{ electrons/cm}^3.$$

The changes in slope approximate changes required to cause the exponential profile to join smoothly with other model profiles. Calculations were performed to show sensitivity to values chosen for h_ℓ and h_u.

Table 11 shows the results for the nighttime calculations. The results show the four components of the anisotropic reflection coefficient calculation for a frequency of 30 kHz and 3 different real incident angles. The reflection coefficient amplitude components are:

Table 11. Reflection coefficients as a function of break points in the exponential profile, $\beta = 0.7$, $h_w = 88$, frequency = 30 kHz.

Upper Break Altitude (km)	Lower Break Altitude (km)	Angle of Incidence (deg)	R11		R22		R21		R12	
100	60	78	5.87E-01	3.51E-02	1.91E-01	-8.27E-01	8.72E-02	3.12E-01	9.32E-02	2.38E-01
		80	5.46E-01	3.56E-01	7.26E-01	-4.85E-01	-1.03E-01	2.66E-01	6.15E-02	2.22E-01
		82	3.29E-01	6.38E-01	8.87E-01	1.46E-01	-2.04E-01	1.28E-01	-1.56E-01	1.21E-01
95	60	78	5.87E-01	3.52E-02	1.90E-01	-8.27E-01	8.73E-02	3.12E-01	9.35E-02	2.38E-01
		80	5.46E-01	3.56E-01	7.25E-01	-4.86E-01	-1.03E-01	2.66E-01	-6.13E-02	2.22E-01
		82	3.28E-01	6.36E-01	8.87E-01	1.45E-01	-2.04E-01	1.28E-01	-1.56E-01	1.21E-01
94	60	78	5.87E-01	3.58E-02	1.84E-01	-8.27E-01	8.81E-02	3.12E-01	9.61E-02	2.40E-01
		80	5.46E-01	3.57E-01	7.21E-01	-4.89E-01	-1.03E-01	2.67E-01	-6.07E-02	2.25E-01
		82	3.28E-01	6.39E-01	8.86E-01	1.41E-01	-2.04E-01	1.29E-01	-1.57E-01	1.24E-01
93	60	78	5.85E-01	3.59E-02	1.63E-01	-8.29E-01	9.36E-02	3.12E-01	1.00E-01	2.44E-01
		80	5.45E-01	3.56E-01	7.10E-01	-5.02E-01	-9.99E-02	2.69E-01	-6.00E-02	2.29E-01
		82	3.28E-01	6.38E-01	8.87E-01	1.28E-01	-2.04E-01	1.32E-01	-1.59E-01	1.27E-01
92	60	78	5.80E-01	3.39E-02	1.08E-01	-8.34E-01	1.10E-01	3.11E-01	1.11E-01	2.48E-01
		80	5.43E-01	3.52E-01	6.80E-01	-5.36E-01	-9.06E-02	2.77E-01	-5.62E-02	2.38E-01
		82	3.29E-01	6.35E-01	8.88E-01	9.17E-02	-2.03E-01	1.40E-01	-1.62E-01	1.34E-01
91	60	78	5.74E-01	3.19E-02	-1.19E-02	-8.34E-01	1.41E-01	3.06E-01	1.37E-01	2.53E-01
		80	5.41E-01	3.47E-01	6.10E-01	-6.05E-01	-7.13E-02	2.91E-01	-4.42E-02	2.57E-01
		82	3.30E-01	6.31E-01	8.86E-01	1.48E-02	-2.00E-01	1.57E-01	-1.66E-01	1.52E-01
90	60	78	5.64E-01	3.54E-02	-2.16E-01	-7.97E-01	1.90E-01	2.85E-01	1.84E-01	2.53E-01
		80	5.35E-01	3.44E-01	4.76E-01	-7.05E-01	-3.59E-02	3.05E-01	-1.84E-02	2.85E-01
		82	3.30E-01	6.26E-01	8.70E-01	-1.15E-01	-1.91E-01	1.81E-01	-1.69E-01	1.82E-01
100	70	78	5.87E-01	3.51E-02	1.91E-01	-8.27E-01	8.72E-02	3.12E-01	9.32E-02	2.38E-01
		80	5.46E-01	3.56E-01	7.26E-01	-4.85E-01	-1.03E-01	2.66E-01	-6.15E-02	2.22E-01
		82	3.29E-01	6.38E-01	8.87E-01	1.46E-01	-2.04E-01	1.28E-01	-1.56E-01	1.21E-01

Table 11. Reflection coefficients as a function of break points in the exponential profile, $\beta = 0.7$, $h_w = 88$, frequency = 30 kHz (Concluded).

Upper Break Altitude (km)	Lower Break Altitude (km)	Angle of Incidence (deg)	R11		R22		R21		R12	
100	75	78	5.87E-01	3.51E-02	1.91E-01	-8.27E-01	8.72E-02	3.12E-01	9.32E-02	2.38E-01
		80	5.46E-01	3.56E-01	7.26E-01	-4.85E-01	-1.03E-01	2.66E-01	-6.15E-02	2.22E-01
		82	3.29E-01	6.38E-01	8.87E-01	1.46E-01	-2.04E-01	1.28E-01	-1.56E-01	1.21E-01
100	76	78	5.86E-01	-4.16E-02	8.18E-02	-8.45E-01	1.27E-01	2.98E-01	1.23E-01	2.24E-01
		80	5.81E-01	2.94E-01	6.68E-01	-5.61E-01	-7.36E-02	2.75E-01	-3.72E-02	2.27E-01
		82	3.83E-01	6.07E-01	8.96E-01	6.75E-02	-1.92E-01	1.45E-01	-1.45E-01	1.34E-01
100	77	78	5.54E-01	-1.91E-01	-1.39E-01	-8.37E-01	1.99E-01	2.55E-01	1.77E-01	1.85E-01
		80	6.29E-01	1.61E-01	5.31E-01	-6.93E-01	-1.25E-02	2.85E-01	1.23E-02	2.30E-01
		82	4.81E-01	5.30E-01	8.94E-01	-8.94E-02	-1.64E-01	1.76E-01	-1.20E-01	1.57E-01
100	78	78	4.83E-01	-3.26E-01	-3.51E-01	-7.72E-01	2.58E-01	1.95E-01	2.18E-01	1.33E-01
		80	6.46E-01	2.16E-02	3.68E-01	-7.91E-01	4.89E-02	2.80E-01	6.07E-02	2.22E-01
		82	5.63E-01	4.37E-01	8.64E-01	-2.44E-01	-1.31E-01	2.02E-01	-9.17E-02	1.75E-01
100	79	78	3.80E-01	-4.36E-01	-5.39E-01	6.55E-01	2.98E-01	1.22E-01	2.44E-01	7.38E-02
		80	6.30E-01	-1.17E-01	1.87E-01	-8.51E-01	1.07E-01	2.63E-01	1.06E-01	2.04E-01
		82	6.24E-01	3.31E-01	8.07E-01	-3.90E-01	-9.42E-02	2.21E-01	-6.17E-02	1.88E-01
100	80	78	2.51E-01	-5.10E-01	-6.90E-01	-4.93E-01	3.18E-01	4.20E-02	2.54E-01	1.10E-02
		80	5.81E-01	-2.44E-01	-2.17E-03	-8.71E-01	1.60E-01	2.33E-01	1.45E-01	1.78E-01
		82	6.61E-01	2.17E-01	7.25E-01	-5.24E-01	-5.55E-02	2.33E-01	-3.14E-02	1.96E-01
95	70	78	5.87E-01	3.52E-02	1.90E-01	8.27E-01	8.73E-02	3.12E-01	9.35E-02	2.38E-01
		80	5.46E-01	3.56E-01	7.25E-01	-4.86E-01	-1.03E-01	2.66E-01	-6.13E-02	2.22E-01
		82	3.28E-01	6.38E-01	8.87E-01	1.45E-01	-2.04E-01	1.28E-01	-1.56E-01	1.21E-01

R_{11} = vertical incidence - vertical reflection

R_{22} = horizontal incidence - horizontal reflection

R_{12} = vertical incidence - horizontal reflection

R_{21} = horizontal incidence - vertical reflection.

The nighttime reference condition, where it could be easily demonstrated that the changes in slope had no effect, were for an upper break point (h_u) of 100 km and a lower break point (h_ℓ) of 60 km.

It can be seen from the table that raising the lower break point above 75 km or lowering the upper break point below 95 km causes the reflection coefficient to change from the reference condition.

Results from a similar analysis for daytime conditions are shown in Table 12. Here the reference condition is for an upper break point of 75 km and a lower break point of 40 km. The results show that the upper break point could be as low as 70 km and the lower break point as high as 45 km without changing the results.

Thus to reproduce calculations that are made with a fictitious exponential profile at all altitudes, the exponential range must extend over an altitude range of 20 to 30 km.

3.3 NUMERICAL FIT PROCEDURE.

The numerical fit used as an ionosphere model for the SIMBAL program (Section 2-3.2) provides a simple mechanism to adjust electron concentration profiles. The equation (see Equation 18) for electron concentration in undisturbed conditions is

$$N_e = \exp\left(C_e + x \ln Q\right)$$

where the values for C_e and x are determined from fits to data calculated with detailed chemistry models. In the altitude range of interest, x is near 0.5, as expected from the electron dependence on the square root of Q. Several procedures were tested by adjusting C_e and/or Q to obtain the exponential concentration where there is no disturbance and to transition smoothly into the model based on chemistry for a moderate disturbance. The

Table 12. Reflection coefficients as a function of break points in the exponential profile, $\beta = 0.3$, $h_w = 72$, frequency = 30 kHz.

Upper Break Altitude (km)	Lower Break Altitude (km)	Angle of Incidence (deg)	R11		R22		R21		R12	
75	40	78	-1.89E-01	-1.85E-01	-1.54E-01	-1.17E-01	2.76E-02	1.06E-02	2.62E-02	-3.08E-02
		80	6.49E-02	-3.22E-01	2.64E-02	-2.63E-01	4.55E-03	2.85E-02	3.82E-02	5.82E-03
		82	3.77E-01	-1.64E-01	3.13E-01	-1.66E-01	-2.03E-02	1.80E-02	1.51E-02	3.22E-02
74	40	78	-1.89E-01	-1.85E-01	-1.54E-01	-1.17E-01	2.76E-02	1.06E-02	2.62E-02	-3.08E-02
		80	6.49E-02	-3.22E-01	2.64E-02	-2.63E-01	4.54E-03	2.85E-02	3.82E-02	5.82E-03
		82	3.77E-01	-1.64E-01	3.13E-01	-1.66E-01	-2.03E-02	1.80E-02	1.51E-02	3.22E-02
72	40	78	-1.89E-01	-1.85E-01	-1.55E-01	-1.18E-01	2.74E-02	1.06E-02	2.62E-02	-3.05E-02
		80	6.47E-02	-3.22E-01	2.65E-02	-2.64E-01	4.46E-03	2.84E-02	3.80E-02	5.92E-03
		82	3.76E-01	-1.65E-01	3.13E-01	-1.66E-01	-2.02E-02	1.79E-02	1.49E-02	3.22E-02
70	40	78	-1.90E-01	-1.85E-01	-1.56E-01	-1.20E-01	2.69E-02	1.06E-02	2.55E-02	-2.97E-02
		80	6.48E-02	-3.23E-01	2.80E-02	-2.66E-01	4.36E-03	2.81E-02	3.72E-02	5.83E-03
		82	3.77E-01	-1.65E-01	3.15E-01	-1.66E-01	-2.00E-02	1.77E-02	1.46E-02	3.16E-02
68	40	78	-1.88E-01	-1.87E-01	-1.54E-01	-1.26E-01	2.63E-02	1.06E-02	2.36E-02	-2.87E-02
		80	6.63E-02	-3.23E-01	3.27E-02	-2.67E-01	4.17E-03	2.77E-02	3.57E-02	4.91E-03
		82	3.78E-01	-1.64E-01	3.18E-01	-1.63E-01	-1.99E-02	1.75E-02	1.46E-02	3.02E-02
66	40	78	-1.83E-01	-1.87E-01	-1.47E-01	-1.34E-01	2.50E-02	1.07E-02	2.02E-02	-2.81E-02
		80	6.93E-02	-3.19E-01	4.10E-02	-2.65E-01	3.63E-03	2.71E-02	3.39E-02	2.74E-03
		82	3.77E-01	-1.60E-01	3.20E-01	-1.57E-01	-1.98E-02	1.71E-02	1.54E-02	2.81E-02
75	42	78	-1.89E-01	-1.85E-01	-1.54E-01	-1.17E-01	2.76E-02	1.06E-02	2.62E-02	-3.08E-02
		80	6.49E-02	-3.22E-01	2.64E-02	-2.63E-02	4.55E-03	2.85E-02	3.82E-02	5.82E-03
		82	3.77E-01	-1.64E-01	3.13E-01	-1.66E-01	-2.03E-02	1.80E-02	1.51E-02	3.22E-02

Table 12. Reflection coefficients as a function of break points in the exponential profile, $\beta = 0.3$, $h_w = 72$, frequency = 30 kHz (Concluded).

Upper Break Altitude (km)	Lower Break Altitude (km)	Angle of Incidence (deg)	R11		R22		R21		R12	
75	43	78	-1.89E-01	-1.85E-01	-1.54E-01	-1.17E-01	2.76E-02	1.06E-02	2.62E-02	-3.08E-02
		80	6.49E-02	-3.23E-01	2.64E-02	-2.63E-01	4.56E-03	2.85E-02	3.82E-02	5.82E-03
		82	3.77E-01	-1.64E-01	3.13E-01	-1.66E-01	-2.03E-02	1.80E-02	1.51E-01	3.22E-02
75	44	78	-1.63E-01	-2.08E-01	-1.38E-01	-1.36E-01	2.60E-02	1.41E-02	3.00E-02	-2.72E-02
		80	9.99E-02	-3.14E-01	5.51E-02	-2.59E-01	1.42E-03	2.89E-02	3.74E-02	9.95E-03
		82	3.90E-01	-1.31E-01	3.27E-01	-1.38E-01	-2.18E-02	1.62E-02	1.22E-02	3.35E-02
75	45	78	-1.35E-01	-2.28E-02	-1.18E-01	-1.53E-01	2.40E-02	1.74E-02	3.33E-02	-2.30E-02
		80	1.34E-01	-3.01E-01	8.33E-02	-2.51E-01	-1.73E-03	2.89E-02	3.61E-02	1.40E-02
		82	4.01E-01	-9.66E-02	3.38E-01	-1.09E-01	-2.32E-02	1.43E-02	9.28E-03	3.44E-02
72	41	78	-1.89E-01	-1.85E-01	-1.55E-01	-1.18E-01	2.74E-02	1.06E-02	2.62E-02	-3.05E-02
		80	6.47E-02	-3.22E-01	2.65E-02	-2.64E-01	4.46E-03	2.84E-02	3.80E-02	5.92E-03
		82	3.76E-01	-1.65E-01	3.13E-01	-1.66E-01	-2.02E-02	1.79E-02	1.49E-02	3.22E-02
72	42	78	-1.89E-01	-1.85E-01	-1.55E-01	-1.18E-01	2.74E-02	1.06E-02	2.62E-02	-3.05E-02
		80	6.47E-02	-3.22E-01	2.65E-02	-2.64E-01	4.46E-03	2.84E-02	3.80E-02	5.92E-03
		82	3.76E-01	-1.65E-01	3.13E-01	-1.66E-01	-2.02E-02	1.79E-02	1.49E-02	3.22E-02

method selected for nighttime was to adjust the ambient value of Q, (Q_A), at 95 km to match the exponential profile. This can be done while retaining a reasonable value for the production rate. Then for altitudes between 75 and 95 km the electron density is computed from

$$N_e = \exp\ (C_e' + x\ \ell n\ Q)$$

where

$$C_e' = C_e \qquad Q \geq 10 \cdot Q_A$$

$$C_e' = f_q C_x + (1 - f_q) C_e \qquad Q < 10 \cdot Q_A$$

where

$$f_q = 1.11 - \frac{Q}{9Q_A} \qquad \text{and}$$

Q_A = normal (undisturbed) ion production rate (ion pairs/cm^3).

Note that $f_q = 1$ $(C_e' = C_x)$ when $Q = Q_A$ and $f_q = 0$ $(C_e' = C_e)$ when $Q = 10\ Q_A$.

The value C_x is the value of C_e required to reproduce the exponential electron density profile when $Q = Q_A$, ie,

$$C_x = \ell n\ (N_e) - x\ \ell n\ Q_A\ .$$

A similar procedure was used to fit the electron concentration profile over the altitude range from 40 to 75 km for daytime conditions, except that none of the normal values for Q_A were adjusted. This procedure is equivalent to an adjustment in atmospheric chemistry parameters, not production rate, and thus will not increase the sensitivity to weak disturbances. The model reproduces the original model data for Q greater than $10\ Q_A$.

Figures 13 and 14 show the results produced by the simple model. Electron and positive ion concentrations are shown as a function of altitude, parametric in ion production rate produced by high-altitude spread debris. Uniformly spread debris is frequently used to characterize widespread VLF/LF disturbances. The spread debris parameter is

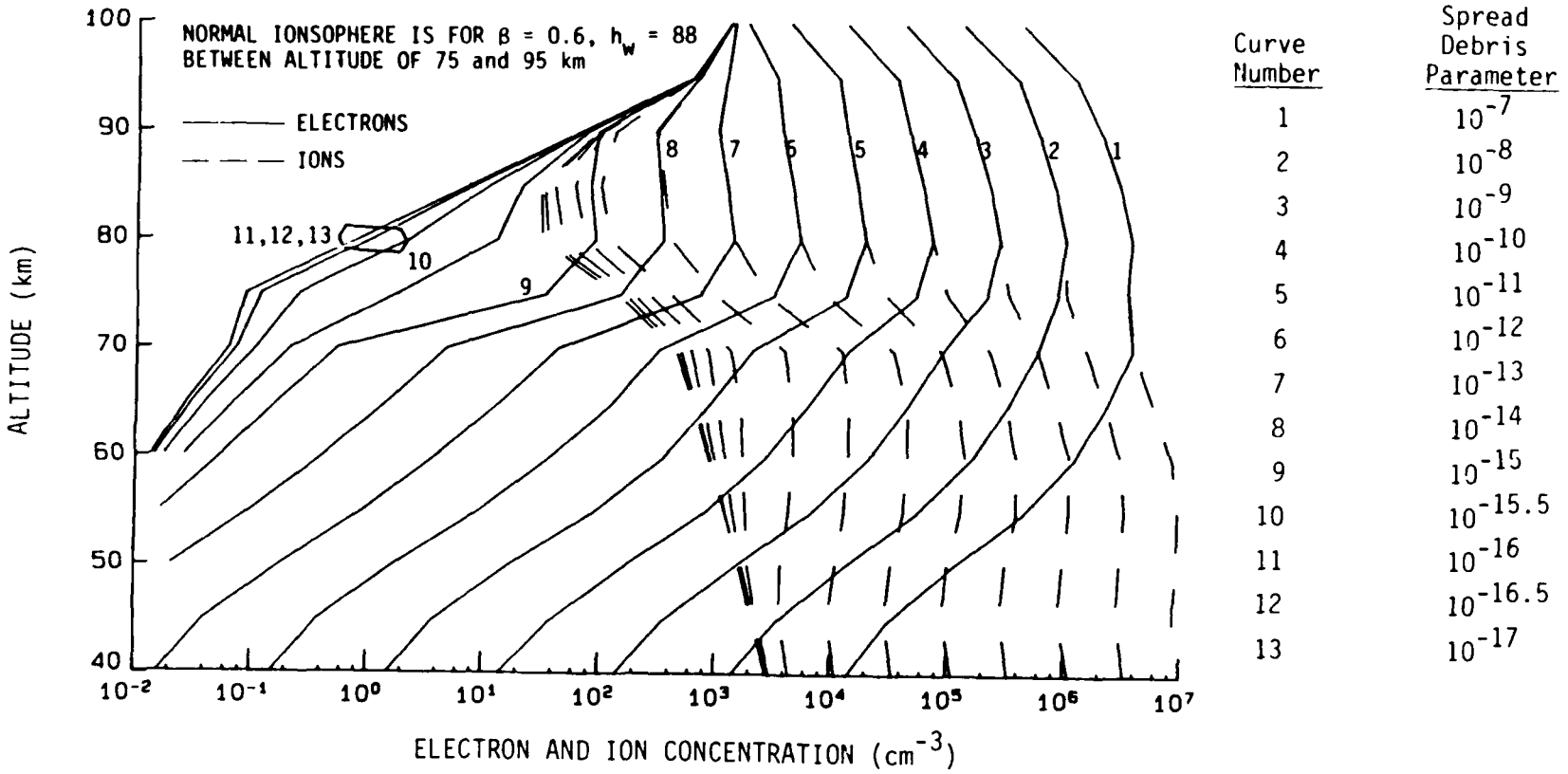

Figure 13. Electron and ion concentration produced by a spread debris source using the SIMBAL modified D-region ionization model (nighttime).

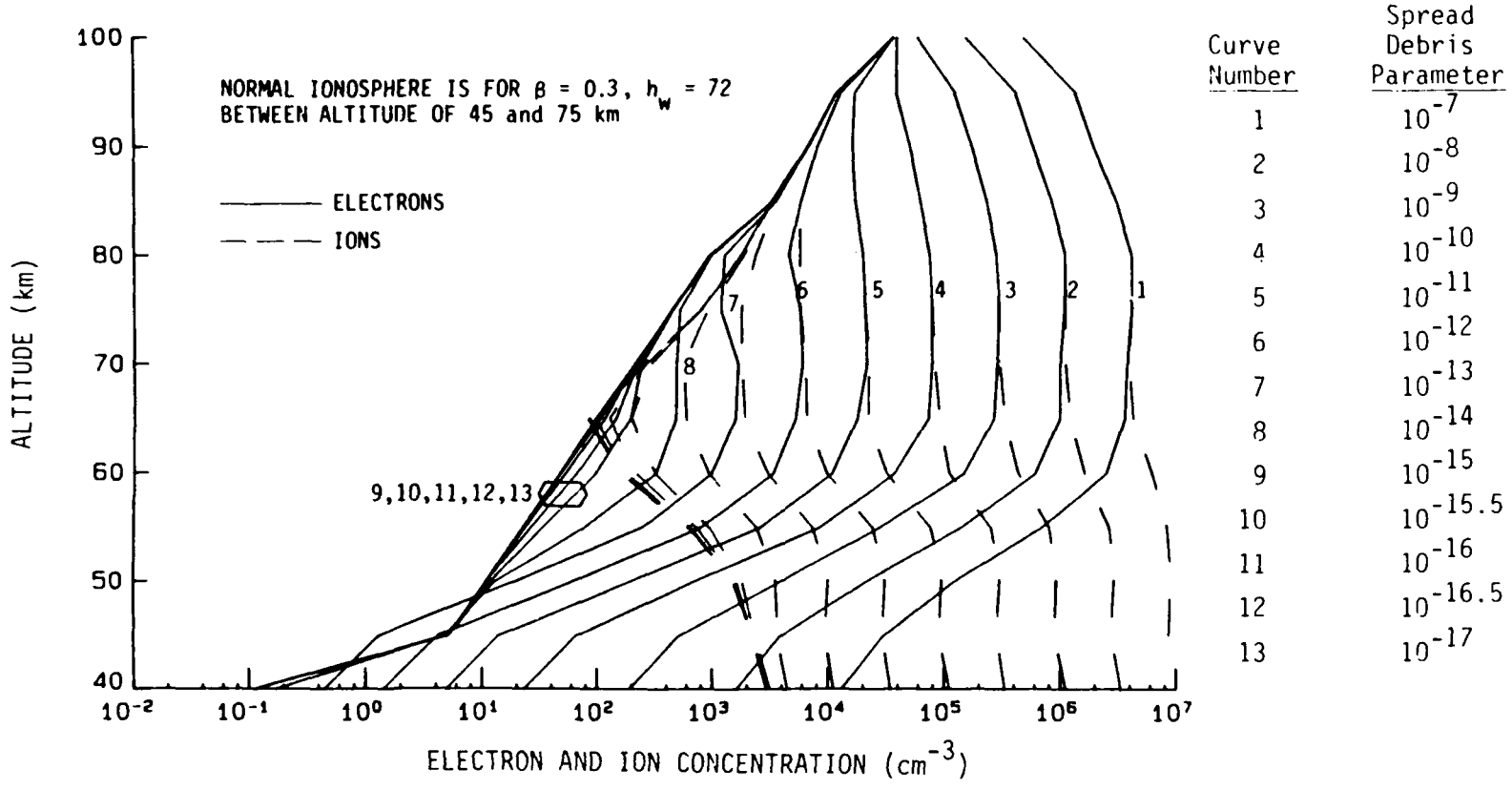

Figure 14. Electron and ion concentration produced by a spread debris source using the SIMBAL modified D-region ionization model (daytime).

$$w = \frac{W_F}{A_d t^{1.2}}$$

where

W_F = fission yield (MT)

A_d = area covered by the high-altitude debris cloud (km^2)

t = time since detonation (sec).

Results are shown for a range of values of w from 10^{-7} (a very intense disturbance) to a value of 10^{-17} (smaller than the normal production rate for both nighttime and daytime conditions). The transition from the exponential for small disturbances is reasonably smooth.

The ion concentration is unchanged from the previous model. One has to be careful in adjusting (reducing) electron concentrations to be sure that the relative effect of ions is not unrealistically increased. The ion and electron concentration curves do not merge at higher altitudes as they should. However, the ion concentration predicted by the model for low Q will not have a significant effect on VLF/LF propagation.

3.4 REACTION RATE AND IONIZATION RATE ADJUSTMENT IN THE WEDCOM CHEMISTRY MODEL.

The lumped parameter chemistry model was briefly described in Section 1. The four lumped-parameter reaction rates (attachment rate, A, detachment rate, D, the ion-ion recombination coefficient, α_i, and the electron-ion recombination coefficient, α_d) are computed using weighted average reactions between several atomic and molecular species in the atmosphere. The species are in equilibrium for a specified normal temperature profile. Arbitrary adjustment of the lumped parameters is similar to the numerical procedure described in Section 3-3. A realistic adjustment requires adjustment of atmospheric species, and changes for one application can cause unwanted changes to the model for other applications. In addition to the complications of adjusting the normal chemistry values, the atmospheric species and the associated reactions are affected by high levels of weapon-produced energy deposition. The weapon-induced changes can be long lasting; thus changes to match preburst conditions do not guarantee recovery to preburst conditions for long periods of time.

The effort described here is not an effort to modify the complex chemistry model. It is a numerical or sensitivity study to indicate the range of values the lumped parameters and ionization rates must have to produce specified profiles.

Emphasis here is placed on nighttime conditions, where the requirement to match propagation data requires reduction of model electron concentration in the 75 to 95 km altitude range. There is a lower limit that can be achieved by simply reducing the ion production rate. This limit is imposed by the maximum decay from realistic daytime values. While any level of quasi-equilibrium electron density can eventually be attained, the actual midnight values are determined by the maximum decay in about a twelve-hour period from daytime conditions. The logical chemistry parameter to vary (Reference 17) is the detachment rate, since the detachment rate varies several orders of magnitude in the altitude range of interest. A change in the altitude distribution of important species (in this case atomic oxygen) can produce orders of magnitude changes in the detachment rate at a specified altitude. (Changes in both attachment and detachment rates which result in the same change in the ratio of A to D would produce results roughly equivalent to those obtained by changing D alone).

Several parametric calculations were performed to test the sensitivity of nighttime electron concentration profiles to changes in Q and D . The calculations were performed in a way to produce a lower limit to the estimated values of nighttime electron values. The procedure was as follows:

1. Set the initial electron and positive ion concentration values to normal noontime values.
2. Assume that the ambient $Q(Q_a)$ and reaction rates are the midnight values.
3. Compute the electron concentration as a function of time.
4. Modify the Q_a's and the detachment rate and repeat 1 through 3.

The calculations were made using Subroutine DTNE (Reference 18) which performs a transient electron concentration calculation for fixed reaction rates. Results were obtained for altitudes of 75, 80, 85, and 90 km and are shown in Figures 15 through 18. The curves all have the same characteristic shape, consistent with the approximate relations in Reference 19 which show the decay from an initial value for no production rate. The electron density quickly decays from the noontime value with an exponential decay according to

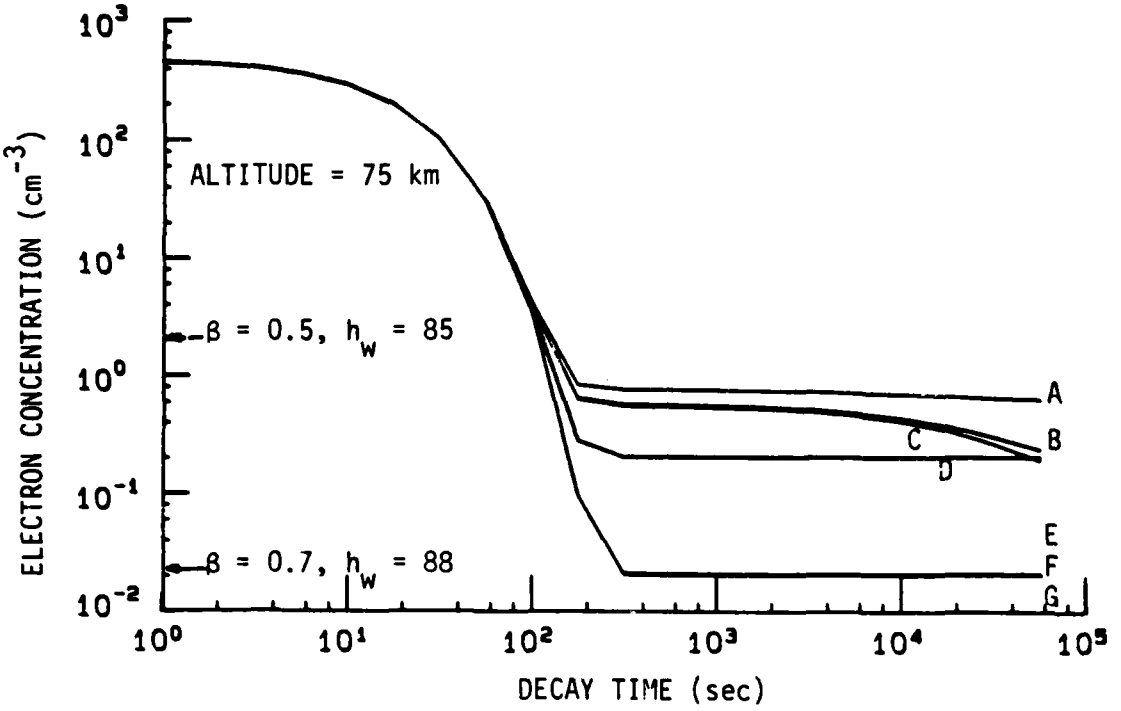

Curve	Ion Production Rate	Detachment Rate
A	10^{-2}	5.76×10^{-5}
B	10^{-3}	5.76×10^{-5}
C	10^{-4}	5.76×10^{-5}
D	10^{-2}	5.76×10^{-8}
E	10^{-2}	5.76×10^{-9}
F	10^{-3}	5.76×10^{-8}
G	10^{-3}	5.76×10^{-9}

Figure 15. Electron decay from noontime conditions at 75 km altitude.

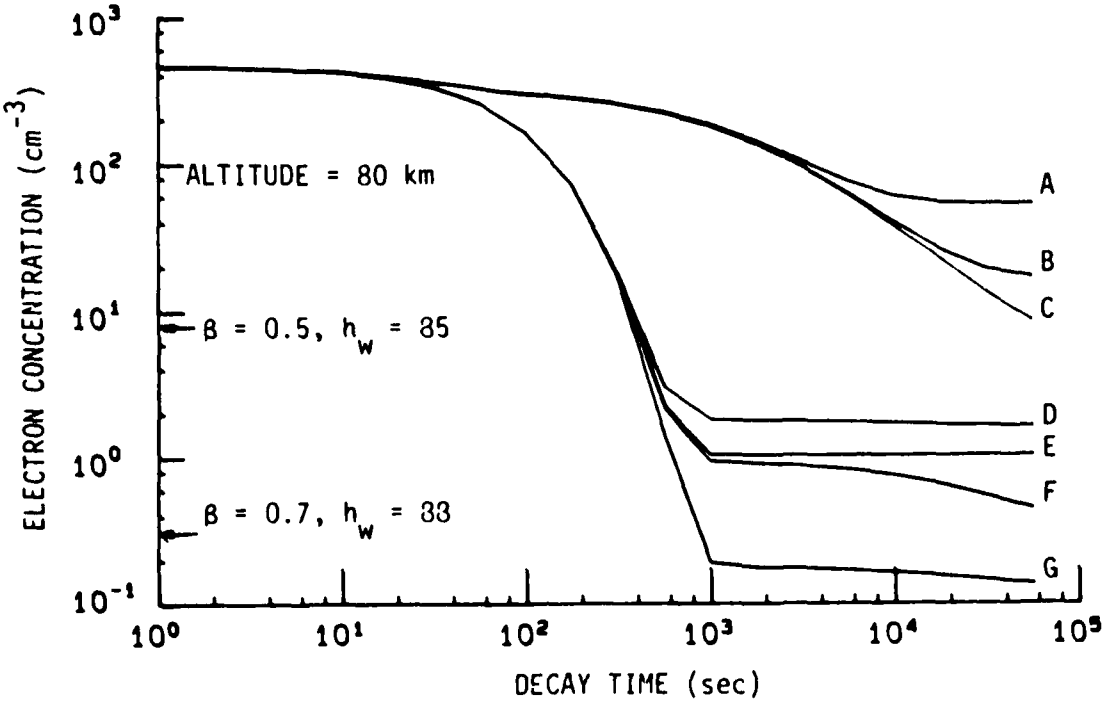

Curve	Ion Production Rate	Detachment Rate
A	10^{-2}	1.93×10^{-2}
B	10^{-3}	1.93×10^{-2}
C	10^{-4}	1.93×10^{-2}
D	10^{-2}	1.93×10^{-5}
E	10^{-2}	1.93×10^{-6}
F	10^{-3}	1.93×10^{-5}
G	10^{-3}	1.93×10^{-6}

Figure 16. Electron decay from noontime conditions at 80 km altitude.

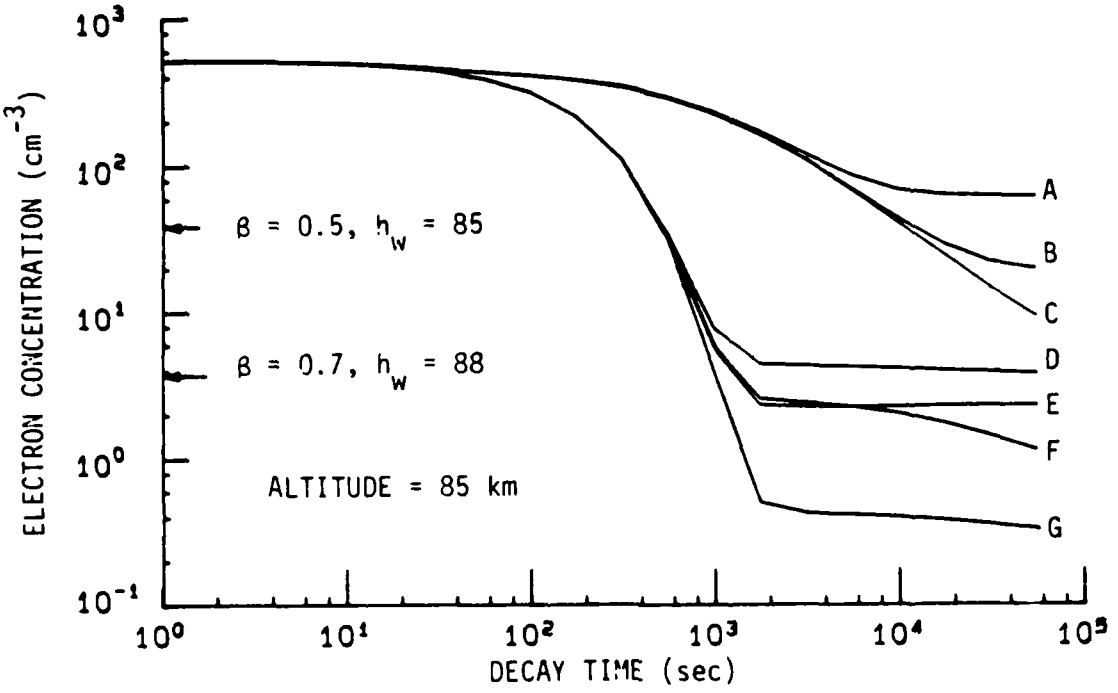

Curve	Ion Production Rate	Detachment Rate
A	10^{-2}	2.39×10^{-2}
B	10^{-3}	2.39×10^{-2}
C	10^{-4}	2.39×10^{-2}
D	10^{-2}	2.39×10^{-5}
E	10^{-2}	2.39×10^{-6}
F	10^{-3}	2.39×10^{-5}
G	10^{-3}	2.39×10^{-6}

Figure 17. Electron decay from noontime conditions at 85 km altitude.

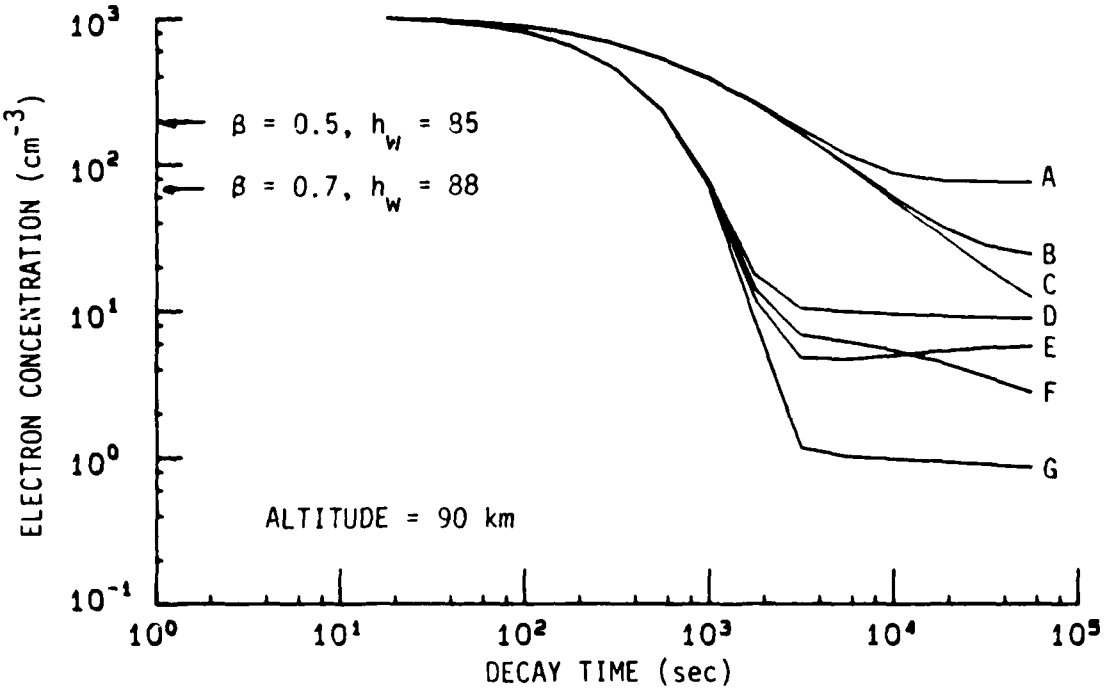

Curve	Ion Production Rate	Detachment Rate
A	10^{-2}	2.16×10^{-2}
B	10^{-3}	2.16×10^{-2}
C	10^{-4}	2.16×10^{-2}
D	10^{-2}	2.16×10^{-5}
E	10^{-2}	2.16×10^{-6}
F	10^{-3}	2.16×10^{-5}
G	10^{-3}	2.16×10^{-6}

Figure 18. Electron decay from noontime conditions at 90 km altitude.

$$N_e(t) \propto e^{-(A+D)t} \quad .$$

The fast decay continues until

$$N_e(t) \simeq \frac{D}{A + D} \frac{N_i}{1 + \alpha N_i t} \quad ,$$

where N_i is the initial value, after which the decay is much slower. Note that the effect of very small ionization rates has no effect until decay time is in excess of 10,000 seconds.

Also shown on the curves for reference are the values of electron concentration that would be computed for the given altitude using exponential profiles with specified values of β and h_w. It can be seen that reducing the value of Q below the nominal values has little effect and that reduction in the detachment rate by a factor of 1000 to 10,000 is required to achieve the electron values for $\beta = 0.7$, $h_w = 88$ at altitudes of 75 and 80 km. At 85 km the reduction required for D is 100 to 1000 and at 90 km no reduction is required.

Figure 19 shows a plot of the WECOM winter-midnight reaction rates. The rapid variation of D in the altitude range of interest is apparent. The dashed curves bracket the values of D required to produce values of electron concentration consistent with the exponential profile with $\beta = 0.7$ and $h_w = 88$. An adjustment in the fraction of atomic oxygen dissociated in the altitude range between 75 and 90 km altitude could produce the change in D (Reference 17). Another mechanism that could be involved is the existence of minor species that dominate the reactions at low ionization levels.

The consistency of such a modification with uncertainties in the model and its impact on other model features requires examination beyond the scope of this effort. Another question is whether such a change, if implemented, should apply for low or all ionization rates. The results do identify a possible model variation that would allow WEDCOM users to choose ionospheric profiles to match selected preburst conditions.

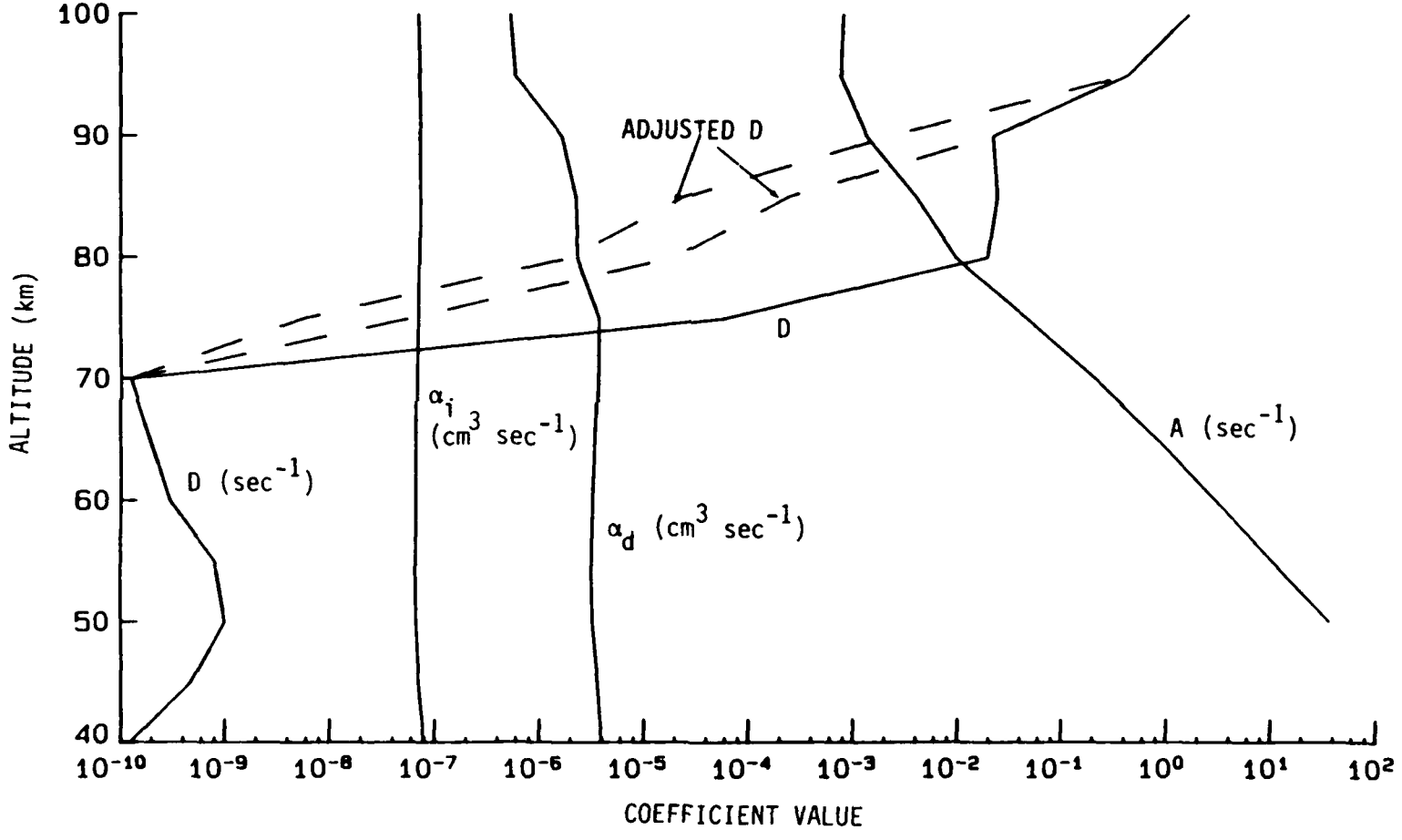

Figure 19. WECOM reaction rates for winter night.

SECTION 4

LIST OF REFERENCES

1. Gambill, B., and R.J. Jordano, SIMBAL: A Fortran Code for Evaluation of the Effects of Multiple Nuclear Weapons on VLF, LF, and HF Communication Links, Volume III: Computational Models, Kaman Tempo (unpublished).

2. Knapp, W.S., and R.R. Rutherford, WEDCOM 85: A Fortran Code for the Calculation of ELF, VLF, and LF Propagation in a Nuclear Environment, Volume I: User's Manual, Kaman Tempo (unpublished).

3. Field, E.C., and R.D. Engle, Detection of Daytime Nuclear Bursts Below 150 km by Prompt VLF Phase Anomalies, Proc. IEEE 53, no. 12, 2009-2017, 1965.

4. Booker, H.G., J.A. Fejer, and K.F. Lee, A Theorem Concerning Reflection from a Plane Stratified Medium, Radio Science 3 (New Series), no. 3, 207-212, 1968.

5. Rutherford, R.R., and B. Gambill, Balloon Gateway Communication Trade-off Studies; VLF/LF/MF Computer Code Modifications, GE80TMP-32, General Electric Company--TEMPO, June 1980.

6. Morfitt, D.G., Effective Electron Density Distributions Describing VLF/LF Propagation Data, NOSC Technical Report 141 (TR 141), Naval Ocean Systems Center, September 1977.

7. Davis, R.M., Jr., and L.A. Berry, A Revised Model of the Electron Density in the Lower Ionosphere, Technical Report TR 111-77, Command & Control Technical Center, Defense Communications Agency, February 1977.

8. McNamara, L.F., Statistical Model of the D Region, Radio Science 14, no. 6, 1165-1173, 1979.

9. Knapp, W.S., Status Report on WEPH Code Modeling - 1978, DNA 4688F, GE78TMP-69, General Electric Company--TEMPO, November 1978.

10. Knapp, W.S., Environment Models for Mid-Level Weapon Effects Communication (WECOM) Codes, KT-85-018(R), Kaman Tempo (unpublished).

11. Finn, R., R.J. Jordano, and W.S. Knapp, The ROSCOE Manual, Volume 11-1--Atmospheric Chemistry Models, GE78TMP-52, General Electric Company--TEMPO, June 1978.

12. W.S. Knapp, and K. Schwartz, WEPH VI: A Fortran Code for the Calculation of Ionization and Absorption Due to Nuclear Detonations, Volume 1, User's Manual, DNA 3766T-1 GE75TMP-53, General Electric Company-TEMPO, September 1975.

13. Knapp, W.S., et al, Weapon Output, Energy Deposition, and Atmospheric Chemistry Models for ROSCOE, Volume I: Atmospheric Chemistry Models, GE74TMP-59, General Electric Company--TEMPO, December 1974.

14. Gambill, B., VLFSIM Link Performance Model, Volume II: Technical Description of Revised Submodels, KT-84-002(R), Kaman Tempo, February 1984 (unpublished).

15. Teters, L.R., et al, Estimating the Performance of Telecommunication Systems Using the Ionospheric Transmission Channel, Ionospheric Communications Analysis and Prediction Program User's Manual, NTIA Report 83-127, U.S. Department of Commerce, July 1983.

16. Chiu, Y.T., An Improved Phenomenological Model of Ionospheric Density, J. Atmos. and Terr. Physics 37, 1563-1570, 1975.

17. Knapp, W.S., private communication, August 1985.

18. Bogusch, R.L., Approximate Series Solutions for the Three-Species Atmospheric Deionization Differential Equations, DASA 1597, 65TMP-7, General Electric Company--TEMPO, February 1965.

19. Knapp, W.S., and K. Schwartz, Aids for the Study of Electromagnetic Blackout, DNA 3499H, GE74TMP-33, General Electric Company--TEMPO, February 1975.

DISTRIBUTION LIST

DEPARTMENT OF DEFENSE

ASST SECY OF DEF CMD CONT COMM & INTEL
ATTN: DASD(I)

ASSISTANT TO THE SECRETARY OF DEFENSE
ATTN: EXECUTIVE ASSISTANT

DEFENSE ADVANCED RSCH PROJ AGENCY
ATTN: GSD R ALEWINE
ATTN: T TETHER

DEFENSE COMMUNICATIONS ENGINEER CENTER
ATTN: CODE R123 TECH LIB
ATTN: CODE R410
ATTN: CODE R410 N JONES

DEFENSE INTELLIGENCE AGENCY
ATTN: RTS-2B

DEFENSE NUCLEAR AGENCY
3 CYS ATTN: RAAE
ATTN: RAAE K SCHWARTZ
ATTN: RAAE P LUNN
ATTN: STNA
4 CYS ATTN: STTI-CA

DEFENSE TECHNICAL INFORMATION CENTER
12 CYS ATTN: DD

FIELD COMMAND DNA DET 2
LAWRENCE LIVERMORE NATIONAL LAB
ATTN: FC-1

FIELD COMMAND DEFENSE NUCLEAR AGENCY
ATTN: FCTT W SUMMA
ATTN: FCTXE

JOINT CHIEFS OF STAFF
ATTN: C3S EVAL OFFICE (HDOO)

JOINT STRAT TGT PLANNING STAFF
ATTN: JLAA
ATTN: JLK (ATTN: DNA REP)
ATTN: JLKS
ATTN: JPTM
ATTN: JPTP

NATIONAL SECURITY AGENCY
ATTN: B432 C GOEDEKE

STRATEGIC DEFENSE INITIATIVE ORGANIZATION
ATTN: KE
ATTN: SLKT
ATTN: SN
ATTN: SY

UNDER SECY OF DEF FOR RSCH & ENGRG
ATTN: STRAT & SPACE SYS (OS)

DEPARTMENT OF THE ARMY

HARRY DIAMOND LABORATORIES
2 CYS ATTN: SCHLD-NW-P

U S ARMY ATMOSPHERIC SCIENCES LAB
ATTN: SLCAS-AE-E

U S ARMY FOREIGN SCIENCE & TECH CTR
ATTN: DRXST-SD

U S ARMY INFO SYS ENGINEERING SUP ACT
ATTN: ASBH-SET-D W NAIR

U S ARMY MATERIAL COMMAND
ATTN: DRCLDC J BENDER

U S ARMY NUCLEAR & CHEMICAL AGENCY
ATTN: LIBRARY

U S ARMY SATELLITE COMM AGENCY
ATTN: AMCPM-SC-3

U S ARMY STRATEGIC DEFENSE CMD
ATTN: DASD-H-SAV
ATTN: DASD-H-SAV R C WEBB

U S ARMY STRATEGIC DEFENSE COMMAND
ATTN: ATC-O W DAVIES
ATTN: ATC-R D RUSS
ATTN: ATC-R W DICKSON

U S ARMY TRADOC SYS ANALYSIS ACTVY
ATTN: ATAA-PL

US ARMY MISSILE COMMAND
ATTN: DRSMI-YSO J GAMBLE

US ARMY WHITE SANDS MISSILE RANGE
ATTN: STEWS-TE-N K CUMMINGS

DEPARTMENT OF THE NAVY

NAVAL ELECTRONICS ENGRG ACTVY, PACIFIC
ATTN: CODE 250 D OBRYHIM

DEPARTMENT OF THE NAVY (CONTINUED)

NAVAL INTELLIGENCE SUPPORT CTR
ATTN: NISC-50

NAVAL OCEAN SYSTEMS CENTER
ATTN: CODE 532
ATTN: CODE 54 J FERGUSON

NAVAL RESEARCH LABORATORY
ATTN: CODE 4180 J GOODMAN
ATTN: CODE 4700 S OSSAKOW
ATTN: CODE 4720 J DAVIS

OFC OF THE DEPUTY CHIEF OF NAVAL OPS
ATTN: NOP 941D

SPACE & NAVAL WARFARE SYSTEMS CMD
ATTN: CODE 501A
ATTN: PDE-110-X1 B KRUGER
ATTN: PDE-110-11021 G BRUNHART
ATTN: PME 106-4 S KEARNEY
ATTN: PME 117-20

STRATEGIC SYSTEMS PROGRAMS(PM-1)
ATTN: NSP-L63 TECH LIB
ATTN: NSP-2141
ATTN: NSP-2722

THEATER NUCLEAR WARFARE PROGRAM OFC
ATTN: PMS-42331F D SMITH

DEPARTMENT OF THE AIR FORCE

AIR FORCE CTR FOR STUDIES & ANALYSIS
ATTN: AFCSA/SASC

AIR FORCE GEOPHYSICS LABORATORY
ATTN: CA A STAIR
ATTN: LIS J BUCHAU
ATTN: LS
ATTN: LS R O'NIEL
ATTN: LSI H GARDINER

AIR FORCE SPACE DIVISION
ATTN: YA
ATTN: YG
ATTN: YK
2 CYS ATTN: YN

AIR FORCE SPACE TECHNOLOGY CENTER
ATTN: XP

AIR FORCE TECHNICAL APPLICATIONS CTR
ATTN: TN

AIR FORCE WEAPONS LABORATORY, AFSC
ATTN: D H HILLAND
ATTN: SUL

AIR FORCE WRIGHT AERONAUTICAL LAB/AAAD
ATTN: A JOHNSON
ATTN: W HUNT

AIR UNIVERSITY LIBRARY
ATTN: AUL-LSE

DEPUTY CHIEF OF STAFF/AFRDS
ATTN: AFRDS SPACE SYS & C3 DIR

ROME AIR DEVELOPMENT CENTER, AFSC
ATTN: TSLD

STRATEGIC AIR COMMAND/NRI-STINFO
ATTN: NRI/STINFO

DEPARTMENT OF ENERGY

DEPARTMENT OF ENERGY
ATTN: DP-233

EG&G, INC
ATTN: D WRIGHT

UNIVERSITY OF CALIFORNIA
LAWRENCE LIVERMORE NATIONAL LAB
ATTN: L-31 R HAGER
ATTN: L-53 TECH INFO DEPT LIB

LOS ALAMOS NATIONAL LABORATORY
ATTN: D SAPPENFIELD
ATTN: D SIMONS
ATTN: J WOLCOTT
ATTN: MS J ZINN
ATTN: R JEFFRIES
ATTN: R W WHITAKER ESS-5
ATTN: T KUNKLE ESS-5

SANDIA NATIONAL LABORATORIES
ATTN: C N VITTITOE
ATTN: D DAHLGREN
ATTN: ORG 1231 T P WRIGHT
ATTN: ORG 314 W D BROWN
ATTN: ORG 332 R C BACKSTROM

OTHER GOVERNMENT

CENTRAL INTELLIGENCE AGENCY
ATTN: OSWR/NED
ATTN: OSWR/SSD FOR K FEUERPFETL

U S DEPARTMENT OF COMMERCE
ATTN: W UTLAUT

DEPARTMENT OF DEFENSE CONTRACTORS

AEROSPACE CORP
ATTN: D OLSEN
ATTN: E RODRIGUEZ
ATTN: I GARFUNKEL

DEPT OF DEFENSE CONTRACTORS (CONTINUED)

AEROSPACE CORP (CONTINUED)
ATTN: J STRAUS
ATTN: R SLAUGHTER
ATTN: V JOSEPHSON

AUSTIN RESEARCH ASSOCIATES
ATTN: J THOMPSON

BERKELEY RSCH ASSOCIATES, INC
ATTN: C PRETTIE
ATTN: J WORKMAN
ATTN: S BRECHT

BOEING CO
ATTN: M/S 6K-92 D CLAUSON

CALIFORNIA RESEARCH & TECHNOLOGY, INC
ATTN: M ROSENBLATT

CORNELL UNIVERSITY
ATTN: D FARLEY JR
ATTN: M KELLY

EOS TECHNOLOGIES, INC
ATTN: B GABBARD
ATTN: W LELEVIER

GEO CENTERS, INC
ATTN: E MARRAM

GTE GOVERNMENT SYSTEMS CORPORATION
ATTN: A MURPHY

HARRIS CORP
ATTN: E KNICK

HSS, INC
ATTN: D HANSEN

INSTITUTE FOR DEFENSE ANALYSES
ATTN: E BAUER

JAYCOR
ATTN: J SPERLING

JOHNS HOPKINS UNIVERSITY
ATTN: C MENG
ATTN: K POTOCKI

KAMAN SCIENCES CORP
ATTN: E CONRAD

KAMAN TEMPO
2 CYS ATTN: B GAMBILL
ATTN: DASIAC
ATTN: W MCNAMARA

KAMAN TEMPO
ATTN: DASIAC

LOCKHEED MISSILES & SPACE CO, INC
ATTN: J KUMER
ATTN: R SEARS

LOCKHEED MISSILES & SPACE CO, INC
2 CYS ATTN: D CHURCHILL

M I T LINCOLN LAB
ATTN: D TOWLE L-230

MAXIM TECHNOLOGIES, INC
ATTN: J LEHMAN
ATTN: J MARSHALL
ATTN: J SO
ATTN: R MORGANSTERN

MCDONNELL DOUGLAS CORP
ATTN: R HALPRIN

METEOR COMMUNICATIONS CORP
ATTN: R LEADER

MISSION RESEARCH CORP
ATTN: C LAUER
ATTN: D KNEPP
ATTN: F FAJEN
ATTN: F GUIGLIANO
ATTN: G MCCARTOR
ATTN: R BIGONI
ATTN: R BOGUSCH
ATTN: R DANA
ATTN: R HENDRICK
ATTN: R KILB
ATTN: S GUTSCHE
ATTN: TECH LIBRARY

MITRE CORP
ATTN: MS J104/M R DRESP

MITRE CORP
ATTN: J WHEELER
ATTN: R C PESCI
ATTN: W FOSTER

PACIFIC-SIERRA RESEARCH CORP
ATTN: H BRODE, CHAIRMAN SAGE

PHOTOMETRICS, INC
ATTN: I L KOFSKY

PHYSICAL DYNAMICS, INC
ATTN: E FREMOUW

PHYSICAL RESEARCH, INC
ATTN: R DELIBERIS
ATTN: T STEPHENS

PHYSICAL RESEARCH, INC
ATTN: J DEVORE
ATTN: J THOMPSON
ATTN: W SCHLUETER

DEPT OF DEFENSE CONTRACTORS (CONTINUED)

R & D ASSOCIATES
ATTN: B LAMB
ATTN: F GILMORE
ATTN: M GANTSWEG
ATTN: W KARZAS

R & D ASSOCIATES
ATTN: B WEBSTER

R & D ASSOCIATES
ATTN: G GANONG

RAND CORP
ATTN: C CRAIN
ATTN: E BEDROZIAN
ATTN: P DAVIS

RAND CORP
ATTN: B BENNETT

SCIENCE APPLICATIONS INTL CORP
ATTN: D HAMLIN
ATTN: L LINSON

SCIENCE APPLICATIONS INTL CORP
ATTN: J COCKAYNE

SCIENCE APPLICATIONS INTL CORP
ATTN: D TELAGE
ATTN: M CROSS

SRI INTERNATIONAL
ATTN: C RINO
ATTN: D MCDANIEL
ATTN: G SMITH
ATTN: J VICKREY
ATTN: R LEADABRAND
ATTN: R TSUNODA
ATTN: W CHESNUT
ATTN: W JAYE

TECHNOLOGY INTERNATIONAL CORP
ATTN: W BOQUIST

TELECOMMUNICATIONS SCIENCES ASSOCIATES
ATTN: J BUCKNER

TOYON RESEARCH CORP
ATTN: J GARBARINO
ATTN: J ISE

TRW ELECTRONICS & DEFENSE SECTOR
ATTN: R PLEBUCH HARD & SURV LAB

UTAH STATE UNIVERSITY
ATTN: A STEED
ATTN: D BURT

VISIDYNE, INC
ATTN: J CARPENTER